AFWL-TR-77-234 Add.

AFWL-TR-77-234 Add.

ADVANCED LASER CONCEPTS

Addendum

TRW
Defense & Space Systems Group
Redondo Beach, CA 90278

May 1979

Final Report

Approved for public release; distribution unlimited.

AIR FORCE WEAPONS LABORATORY
Air Force Systems Command
Kirtland Air Force Base, NM 87117

AFWL-TR-77-234 Add.

This addendum was prepared by TRW, Defense and Space Systems Group, Redondo Beach, California, under Contract F29601-76-C-0065, Job Order 12560309. Mr D. J. Benard was the Laboratory Project Officer-in-Charge.

When US Government drawings, specifications, or other data are used for any purpose other than a definitely related Government procurement operation, the Government thereby incurs no responsibility nor any obligation whatsoever, and the fact that the Government may have formulated, furnished, or in any way supplied the said drawings, specifications, or other data is not to be regarded by implication or otherwise as in any manner licensing the holder or any other person or corporation or conveying any rights or permission to manufacture, use, or sell any patented invention that may in any way be related thereto.

This report has been authored by a contractor of the US Government. Accordingly, the US Government retains a nonexclusive royalty-free license to publish or reproduce the material contained herein, or allow others to do so, for the US Government purposes.

This report has been reviewed by the Office of Information (OI) and is releasable to the National Technical Information Service (NTIS). At NTIS it will be available to the general public, including foreign nationals.

This addendum has been reviewed and is approved for publication.

David J. Benard

DAVID J. BENARD
Project Officer

David S. Olson

DAVID S. OLSON
Lt Col, USAF
Chief, Chemical Laser Branch

FOR THE COMMANDER

Armand D. Maio

ARMAND D. MAIO
Col, USAF
Chief, Advanced Laser Tech Division

DO NOT RETURN THIS COPY. RETAIN OR DESTROY.

UNCLASSIFIED

SECURITY CLASSIFICATION OF THIS PAGE (When Data Entered)

REPORT DOCUMENTATION PAGE

READ INSTRUCTIONS BEFORE COMPLETING FORM

1. REPORT NUMBER: AFWL-TR-77-234-Add	2. GOVT ACCESSION NO.
3. RECIPIENT'S CATALOG NUMBER: Final Rept.	
4. TITLE (and Subtitle): ADVANCED LASER CONCEPTS. Addendum. Production of NF excited States.	5. TYPE OF REPORT & PERIOD COVERED: Sept 76 - Dec 77, Addendum
	6. PERFORMING ORG. REPORT NUMBER
7. AUTHOR(s): D. J. Miller	8. CONTRACT OR GRANT NUMBER(s): F29601-76-C-0065, ARPA Order-2861
9. PERFORMING ORGANIZATION NAME AND ADDRESS: TRW, Defense & Space Systems Group, One Space Park, Redondo Beach, CA 90278	10. PROGRAM ELEMENT, PROJECT, TASK AREA & WORK UNIT NUMBERS: 62301E / 12560309
11. CONTROLLING OFFICE NAME AND ADDRESS: Air Force Weapons Laboratory (ALC), Kirtland Air Force Base, NM 87117	12. REPORT DATE: May 1979
	13. NUMBER OF PAGES: 90
14. MONITORING AGENCY NAME & ADDRESS (if different from Controlling Office): 191p.	15. SECURITY CLASS. (of this report): UNCLASSIFIED
	15a. DECLASSIFICATION/DOWNGRADING SCHEDULE

16. DISTRIBUTION STATEMENT (of this Report)

Approved for public release; distribution unlimited. 62301E

17. DISTRIBUTION STATEMENT (of the abstract entered in Block 20, if different from Report)

18. SUPPLEMENTARY NOTES

19. KEY WORDS (Continue on reverse side if necessary and identify by block number)

Chemical Electronic Transition Laser
Laser Nozzle
Nitrogen Fluoride
Staged Combustion Nozzle
Tetrafluorohydrazine
Tristream Laser Nozzle
a 1 Delta b 1 Sigma +

20. ABSTRACT (Continue on reverse side if necessary and identify by block number)

Experiments are described which use an exclusively chemical system to generate the necessary reagents and energy transfer partners required for production of the $a^1\Delta$ and $b^1\Sigma^+$ electronic excited states of the NF molecule. The purpose is to assess the potential for the development of an electronic transition chemical laser operating on the NF ~~($a^1\Delta \rightarrow X^3\Sigma^-$) or NF ($b^1\Sigma^+ \rightarrow X^3\Sigma^-$)~~ transitions at wavelengths of 874 nm or 529 nm, ~~respectively.~~ In the first of these experiments, staged combustion in a laser cavity is employed by adding a second mixer downstream from the cavity mixer in a conventional, supersonic, diffusion mixing HF

→ next page

DD FORM 1 JAN 73 1473 EDITION OF 1 NOV 65 IS OBSOLETE

UNCLASSIFIED

SECURITY CLASSIFICATION OF THIS PAGE (When Data Entered)

409637

chemical laser. This allows for the mixing of F-atoms, H_2, and N_2F_4 the starting reagents required in the NF system. The second set of experiments utilized a tristream HF chemical laser nozzle which allows the three reagents F-atoms, H_2, and N_2F_4 to be mixed in the throat of a supersonic slit nozzle. In both sets of experiments, thermal dissociation of N_2F_4 was the limitation for the final concentration of NF excited states. For the staged combustion experiments $NF(a^1\Delta) = 6.8 \times 10^{13}$ molec/cm^3 and $NF(b^1\Sigma^+) = 2.3 \times 10^{12}$ molec/cm^3 at cavity conditions of 6.1 torr, 985 K, and linear flow velocity = 4×10^4 cm/s. In the tristream nozzle experiments $NF(a^1\Delta) = 2.5 \times 10^{14}$ molec/cm^3 and $NF(b^1\Sigma^+) = 5.9 \times 10^{12}$ molec/cm^3 for cavity conditions of 1.1 torr, 730 K, and linear flow velocity = 2.5×10^5 cm/s. In both experiments the quenching of NF excited states is slow.

PREFACE

This final technical report is an addendum to the "Advanced Laser Concepts" report prepared under Contract No. F29601-76-C-0065, ARPA Order No. 2861 for the period 6 April 1976 to 6 December 1977. That previous report was prepared by J. A. Betts and D. J. Miller of TRW Defense and Space Systems Group, Redondo Beach, California and was sponsored by the Advanced Research Projects Agency and monitored by Air Force Weapons Laboratory.

This current report "Advanced Laser Concepts – Production of NF Excited States" is for the period 16 January to 29 July 1978, and deals with the chemical production of electronic excited states of NF. All work under this report was monitored and sponsored by Air Force Weapons Laboratory, Albuquerque, New Mexico under Contract No. F29601-76-C-0065. Capt. Steve Davis, Capt. Russel Armstrong, Lt. Greg Bradburn, and Dr. Dave Bernard all have served as project officer.

The author wishes to express his appreciation to the following individuals for major contributions to this program: F. Alvarez, D. Anthony, J. Betts, and M. Sabety-Dzvonik of TRW and R. Armstrong, G. Bradburn, and S. Davis of AFWL.

The author also wishes to thank J. Friichtenicht and B. Wicke of TRW for many helpful discussions during the course of this work.

Finally, J. Herbelin and M. Kwock of the Aerospace Corp. are acknowledged for their helpful discussions and assistance with the supply of N_2F_4 gas.

CONTENTS

CONTENTS (Continued)

ILLUSTRATIONS

ILLUSTRATIONS (Continued)

ILLUSTRATION (Continued)

TABLES

1. INTRODUCTION

The objective of this program is to study the chemical reactions and energy transfer processes which result in production of the $a^1\Delta$ and $b^1\Sigma^+$ electronic excited states of the NF molecule. The purpose here is to assess the potential for the development of an electronic transition chemical laser operating on the $NF(a^1\Delta \rightarrow X^3\Sigma^-)$ or $NF(b^1\Sigma^+ \rightarrow X^3\Sigma^-)$ transitions at wavelengths of 874 nm or 529 nm respectively. An important principle for this work is the use of an exclusively chemical system to generate the necessary reagents and energy transfer partners required for production of the NF excited states.

The major effort on the previous contract[1] was concentrated on studies of ways of pumping the $A^2\Pi$ state of the CN molecule. The second part of the contract concentrated on studies of the chemical pumping of the $b^1\Sigma^+$ and $a^1\Delta$ state of NF. The work on NF in the contract successfully demonstrated the ability to handle and deliver the N_2F_4 reagent to a laser type device, as well as the ability to detect the NF excited states. The results, however, were not encouraging for the possibility of eventual scaling of the system to a region where NF lasing might be demonstrated. Subsequent experiments using staged combustion in the laser cavity were done under TRW IR&D sponsorship, and the results demonstrated increased $NF(b^1\Sigma^+)$ state number density. These results demonstrated production of NF excited states in a completely chemical, supersonic, diffusion mixing laser.

The experiments done under TRW IR&D sponsorship on the NF system represent the first application of staged combustion to a supersonic, diffusion mixing chemical laser system. Staged combustion is simply the addition of reagents into a chemical laser flow at different distances along the flow axis. Care must be taken to avoid severe aerodynamic disturbances in the supersonic flow stream while maintaining efficient mixing. Aerodynamically shaped blades are used for reagent mixing in this application. Such blades have undergone extensive testing as primary mixing blades in conventional HF chemical lasers.

Staged combustion in a chemical laser is especially applicable to chemical production of NF excited states. The primary pumping reaction is

$$H(^2S) + NF_2(^2B_1) \rightarrow HNF_2^*(^1A) \rightarrow HF(X^1\Sigma^+) + NF(a^1\Delta) \qquad (1)$$

It is well established that reaction (1) is fast and it takes place from ground state reactants to produce ~ 100 percent of excited state $NF(a^1\Delta)$.[2,3] The proposed explanation[4] of this selective process is that the reaction proceeds on an addition-elimination rather than abstraction mechanism path. If the reaction proceeds through a singlet state intermediate, then by conservation of electronic spin, singlet state products are predicted. If the reaction proceeds by direct abstraction, then the ground triplet state $NF(X^3\Sigma^-)$ is anticipated.

A reactive flow analysis[3] has provided a rate coefficient for reaction (1) of $k = 2 \times 10^{13}$ cm^3/mol-sec at 298°K and a value of the radiative lifetime of the $NF(a^1\Delta)$ state to be 0.7 sec for the forbidden transition to the ground electronic states. The (0,0) band for this transition has a violet shaded Q branch head at 874.24 nm.

The NF_2 radical required in reaction (1) can be supplied by thermal decomposition of N_2F_4 at moderate temperatures. The low N-N bond strength in tetrafluorohydrazine results in the presence of detectable amounts of difluoroamino radicals even at ambient temperatures. At 600°K N_2F_4 dissociation is virtually complete at equilibrium.[5] The kinetics of the thermal dissociation of N_2F_4 in the presence of excess inert gas can be written

$$M + N_2F_4 \rightleftarrows M + 2NF_2 \qquad (2)$$

where M is the collision partner. The forward rate constant has been measured for M = Ar or N_2[6], and it is expected that at the temperature and pressure typical of an HF chemical laser cavity, any N_2F_4 injected into the laser cavity will be largely dissociated.

Hydrogen atoms can be more difficult to supply in copious amounts. The bond in H_2 is strong and considerable thermal energy is required to dissociate it. Also if H atoms are required to flow some distance or through intricate mixer hardware, recombination is efficient due to surface interactions. An alternate way to produce H atoms is from the reaction

$$F + H_2 \rightarrow HF(v) + H \qquad (3)$$

This is of course the central reaction in the HF chemical laser. The fluorine atoms required in (3) are easily made by completely chemical means in a conventional combustor, and after expansion through a supersonic nozzle, they are mixed with H_2 cavity fuel to produce H atoms. These H atoms can then flow along to the point where they mix with the NF_2 reagent from the secondary mixer. Staged combustion such as this can allow for the separate production of starting reagents and allow for maximum efficiency in their production. This type of combustor-supersonic nozzle-mixer configuration is a well established technique used in existing chemical lasers, and is very adaptable to scaling to larger dimensions and gas throughput.

It is important to note in the present experiments that reaction (3) produces not only the hydrogen atoms, but also generates the heat in the laser cavity to thermally decompose the N_2F_4 by reaction (2). In this way both the reagents required in the pumping reaction (1) are produced. Reaction (3) also produces vibrationally excited HF(v) required in a subsequent energy transfer reaction.

Chemiluminescence at 528.78 nm from the $b^1\Sigma^+$ state of NF to the ground $X^3\Sigma^-$ state is also observed in H/NF_2 systems.[1,2] The $NF(b^1\Sigma^+)$ is produced from the $NF(a^1\Delta)$ by a V-E energy transfer involving HF

$$HF(v \geq 2) + HF(a^1\Delta) \rightarrow HF(v - 2) + NF(b^1\Sigma^+) + \Delta E \qquad (4)$$

Here ΔE is -309.09 and -30.44 cm^{-1} for HF(2) and HF(3), respectively, assuming the two NF species are in their ground vibrational levels. In these experiments, copious amounts of vibrationally excited HF are produced by reaction (3).

Deuterium atoms are equally effective as hydrogen atoms in producing $NF(a^1\Delta)$ by reaction (1). However, when H_2 is replaced by the same molar flow at D_2, reaction (3) now produces vibrationally excited DF(v) and the $NF(b^1\Sigma^+)$ emission practically disappears. In the D_2 system, the DF(3) and DF(4) have resonance defects of 1000 and 730 cm^{-1} respectively, for a $\Delta v = 3$ V-E energy transfer. The expected lower probability of V-E energy transfer in the DF case supports reaction (3) as the source of $NF(b^1\Sigma^+)$ in

the H_2 system.

An experimental determination[7] has been made for the radiative lifetime of the NF($b^1\Sigma^+$) transition at 528.78 nm, and gives τ = 16 msec. The rate coefficient for reaction (4) is estimated[8] to be k = 1.3 x 10^{12} cm^3/mol-sec for HF(2) and k = 3.4 x 10^{13} cm^3/mol-sec for HF(3) at 298°K. A subsequent theoretical analysis[4] argues that reactions involving the excited NF singlet states are significantly slower than the corresponding reactions involving the ground electronic state. Experimental determination of collisional quenching rates of NF($b^1\Sigma^+$) and ($a^1\Delta$) by such species as HF, H_2, D_2 and H atoms show such processes to be slow.[7] It should be possible to generate large concentration of electronically excited NF($b^1\Sigma^+$) if the required H atoms vibrationally excited HF(v), and NF_2 radicals can be produced. The appropriateness of such a system for a visible wavelength chemical laser are obvious.

Two additional reactions need to be mentioned which involve the emission of N_2 first positive bands. It has been proposed in the NF system[2] that the reactions

$$H(^2S) + NF(a^1\Delta) \rightarrow HF(X^1\Sigma^+) + N^*(^2D) \qquad (5)$$

and

$$N^*(^2D) + NF(a^1\Delta) \rightarrow N_2(B^3\Pi_g) + F(^2P_{1/2}) \qquad (6)$$

produce the observed yellow emission from the $N_2(B^3\Pi_g) \rightarrow (A^3\Sigma_u^+)$ band. The evidence supporting this conclusion is multifold based upon a variety of physical observations, thermodynamic arguments, and level of vibrational excitation in the N_2 spectra. The intensity of N_2 emission observed in these experiments is such that in consideration of its shorter radiative lifetimes ($\tau \sim 5$ μsec) compared to the NF excited states, reactions (5) and (6) probably do not play a major role in the destruction of NF($a^1\Delta$). However, the (2,1) and (1,0) vibrational bands of the N_2 first positive partially mask the NF($a^1\Delta$) 874 nm emission and can make quantitative measurements difficult. Also, since the removal of the $N_2(B^3\Pi_g)$ species is primarily by spontaneous emission at our pressures, the yellow flame indicates the observed lifetime of the NF($a^1\Delta$) as well as the presence of excess

hydrogen atoms. A green flame is indicative of conditions where the $NF(b^1\Sigma^+)$ 529 nm emission dominates.

A large part of the present work deals then with the investigation of the staged combustion concept for production of NF excited states. A small scale (15 watt, cw) conventional supersonic, diffusion mixing HF laser was modified to allow a second mixer to be placed downstream of the primary cavity mixer. In this way N_2F_4 can be mixed in with the supersonic flow of reactive gases in the laser.

The present work also included a substantial effort to produce excited NF using a tri-stream chemical laser nozzle. Most conventional HF chemical laser nozzle/mixers allow for the mixing of two reactive gases at the exit plane of a supersonic nozzle. The tri-stream nozzle (TSN) allows for the mixing of three component gases at the throat of a slit nozzle, prior to substantial expansion. The TSN hardware has previously been used as a DF laser device[9], and was supplied for this contract by AFWL. While the TSN represented a second technique for mixing the three reagents N_2F_4, H_2, and F-atoms, the TSN experiments were also designed to gather data to compare to previous LAMP modeling calculations performed at AFWL for the TSN with the NF system.

Both the staged combustion and TSN experiments represent systems which can produce NF excited states by exclusively chemical means utilizing straight-forward modifications of already established laser techniques. While neither experiment is of a scale to expect lasing from NF, the goal here is to identify key technical issues which need to be addressed in order to determine the scale and characteristics of a possible laser device.

2. STAGED COMBUSTION EXPERIMENTS

This section will describe experimental techniques, apparatus, and results as they pertain to the staged combustion experiments to produce $NF(a^1\Delta)$ and $(b^1\Sigma^+)$ electronic states. Many of the diagnostic, gas handling, and data reduction techniques are the same as those applied in the tri-stream nozzle experiments. The description of those experiments in Section 3.0 will not duplicate the description of similar experimental techniques.

2.1 EXPERIMENTAL

2.1.1 Experimental Apparatus

The apparatus used in the staged combustion experiments consisted of a conventional HF supersonic, diffusion mixing laser with gain length of 3.1 cm. This is the MK-I device and is capable of 10-20 watts of HF cw lasing power. To this laser device a second cavity injector has been added downstream of the usual cavity injector in order to separate the chemical production of hydrogen atoms from that of NF_2, the two primary reagents required for NF excited state production. This staging of chemical combustion at varying distances along the flow axis allows for flexibility in the conditions to produce these reagents, and to maximize the efficiency of NF production. A schematic diagram of the staged combustion system is shown in Figure 1. The laser is constructed in a building block arrangement and its component parts are described below.

2.1.1.1 Combustor

The combustor is of water-cooled aluminum construction with an inside diameter of 4.4 cm. It is closed at one end by the F_2/D_2/He burner shown in Figure 2. Combustor gas flows produce fluorine atoms by thermal dissociation. A pressure tap is located 6.4 cm from the upstream end of the combustor and the overall length from the burner head to the nozzle throat is 31.5 cm.

2.1.1.2 Primary Supersonic Expansion Nozzle

Three different interchangeable nickel nozzles can be used in this device. All are rectangular slot-type supersonic nozzles which are con-

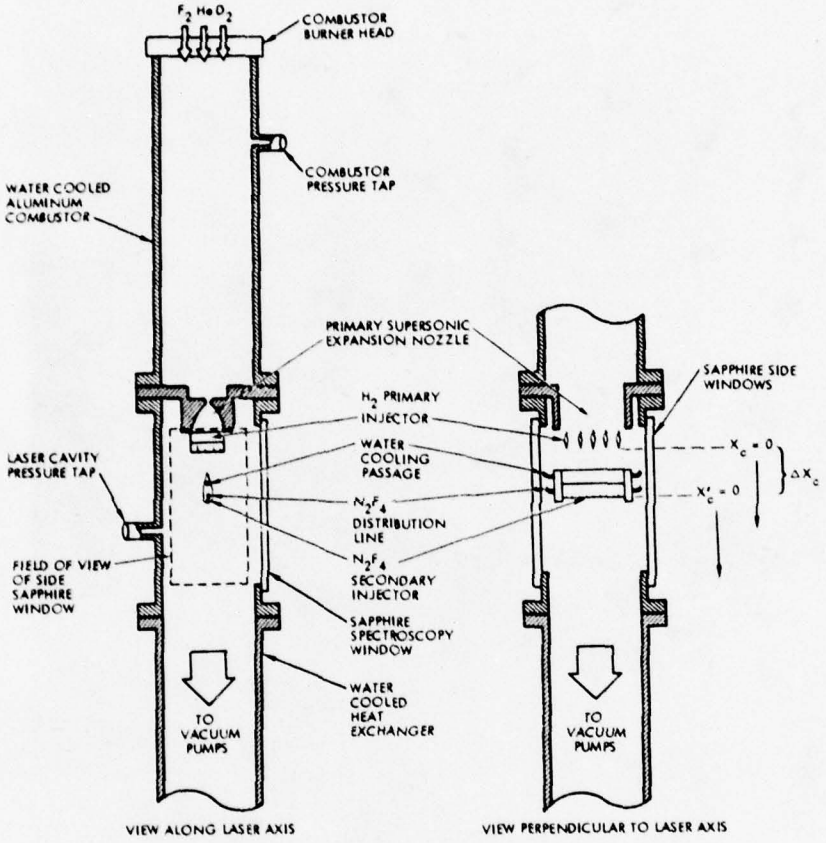

Figure 1. NF Staged Combustion Laser Device.

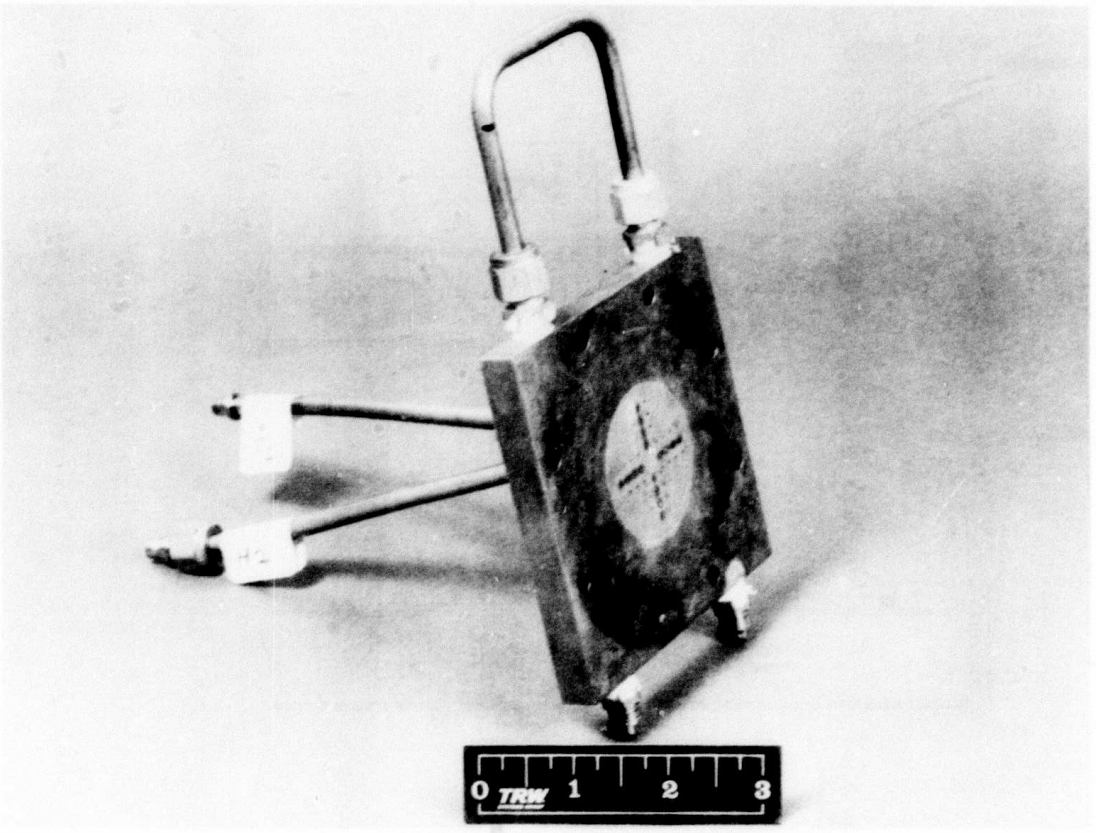

Figure 2. Combustor Burner Head of Water-Cooled Copper Construction. The Scale Is in Inches.

toured for parallel flow. They are 3.1 cm in the gain direction, and are 1.2 cm high at the exit plane. The resulting exit area is 3.72 cm^2. A typical nozzle is shown in Figure 3.

While the exit area remains constant for the three nozzles, they each have different sonic throat heights to give an area expansion ratio of $A/A^* = 4$, 10, or 14. For the $A/A^* = 10$ and 14 nozzles, the sonic throat area was determined by a cold flow experiment using a metered flow of helium gas. This is a more accurate measurement than by geometrically determining the sonic throat area.

2.1.1.3 Primary Injector

Two different copper primary injectors are used to mix hydrogen fuel into the combustor gases expanding from the nozzle. Both are of the Busemann biplane type, and are shown in Figure 4. The two injectors differ only in the number of vanes.

The individual vanes are the same for each injector. They are diamond-shaped, and are 1.2 cm in height and 0.95 cm long in the flow direction. The vane is 0.77 cm wide at its center point. The individual injectors maintain the same exit area of the nozzle. Figure 5 shows the primary injector attached to the nozzle.

The nine-vane injector has four holes of 0.036 cm diameter on the aft end of each vane for the H_2 flow. The five-vane injector also has four holes per vane with a 0.018 cm diameter.

2.1.1.4 Secondary Injector

The secondary injector is downstream from the primary injector and is used to mix N_2F_4 into the HF flow stream. It consists of a single water-cooled nickel blade with a wedge-shaped cross section. Figure 6 shows the individual blade.

The long dimension of the wedged portion of the blade is 2.9 cm and it is positioned along the lasing axis, that is, the blade is perpendicular to the plane of the Busemann vanes.

The blade is 0.68 cm long in the flow direction, and the aft end has ten 0.01 cm diameter holes for N_2F_4 injection.

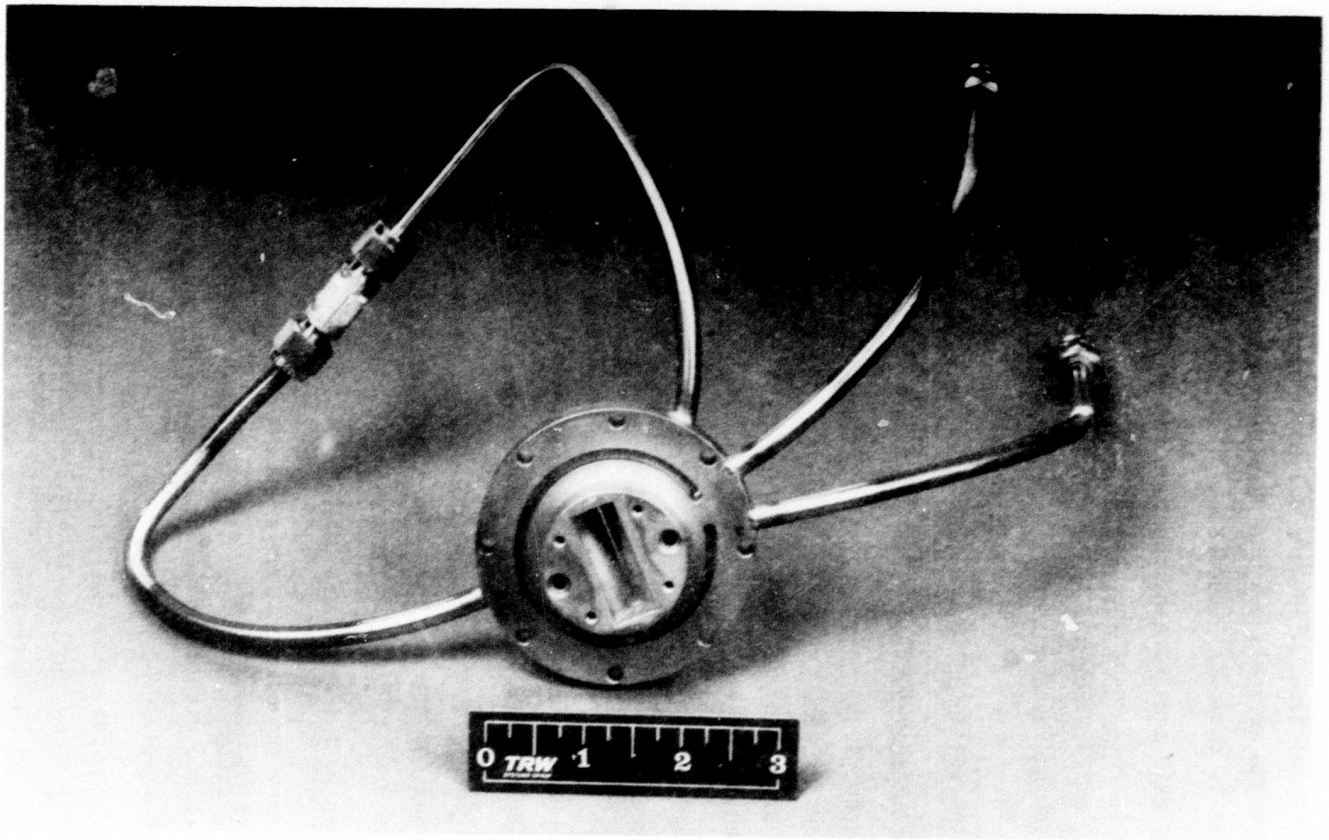

Figure 3. Primary Supersonic Expansion Nozzle (Upstream View). The Exit Area Is 3.1 cm X 1.2 cm = 3.72 cm^2. The Nozzle Is of Water-Cooled Nickel Construction. The Scale Is in Inches.

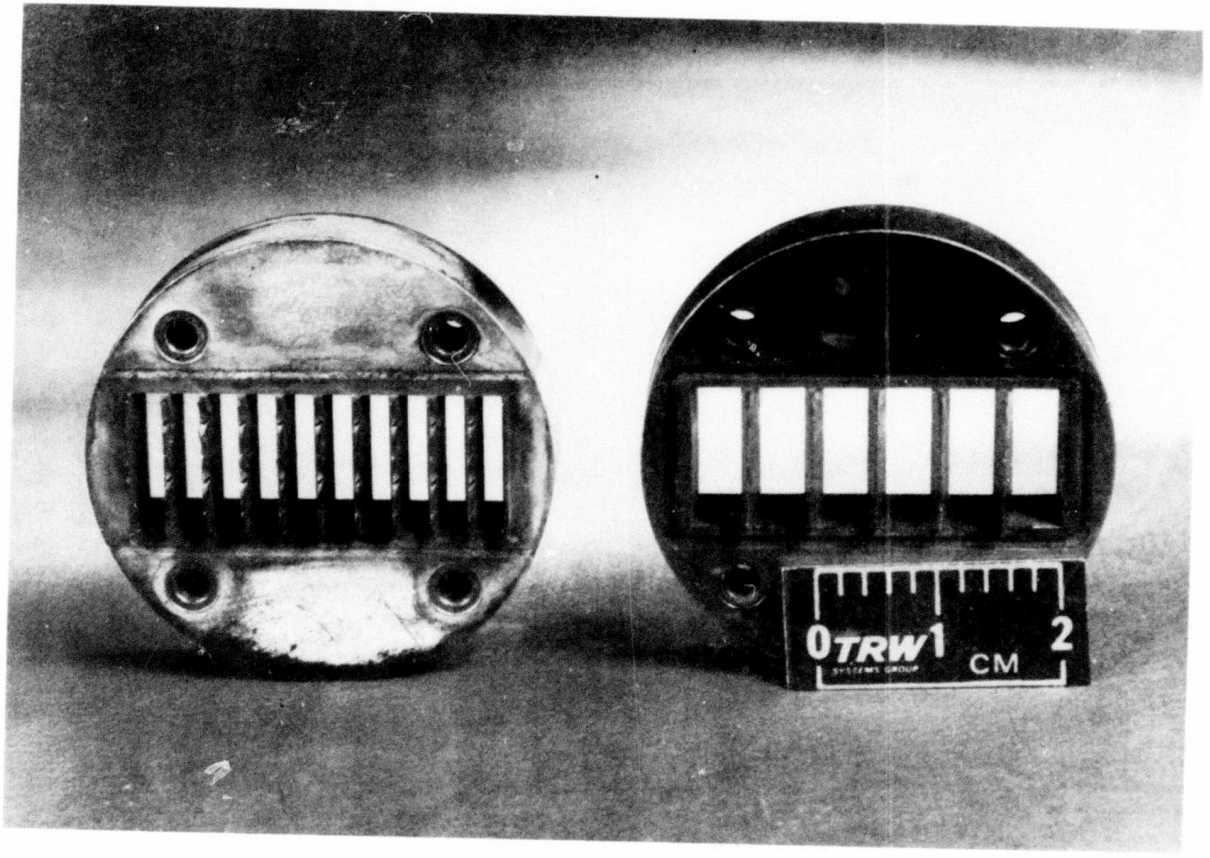

Figure 4. Upstream View of Busemann Biplane Primary Injectors. They Are Constructed From Copper, and the 9-Vane and 5-Vane Version Are Shown.

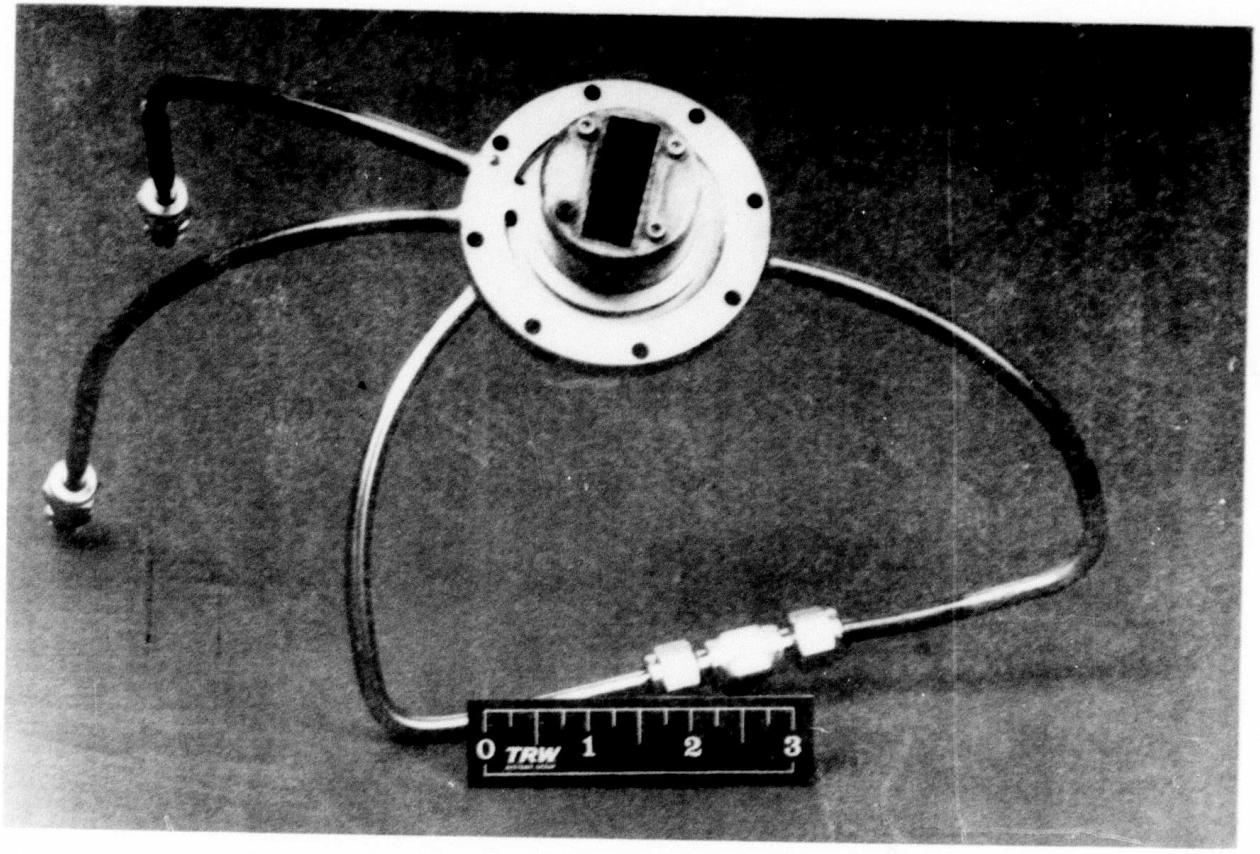

Figure 5. Primary Nozzle With 9-Vane Busemann Biplane Injector Attached. The Scale Is in Inches.

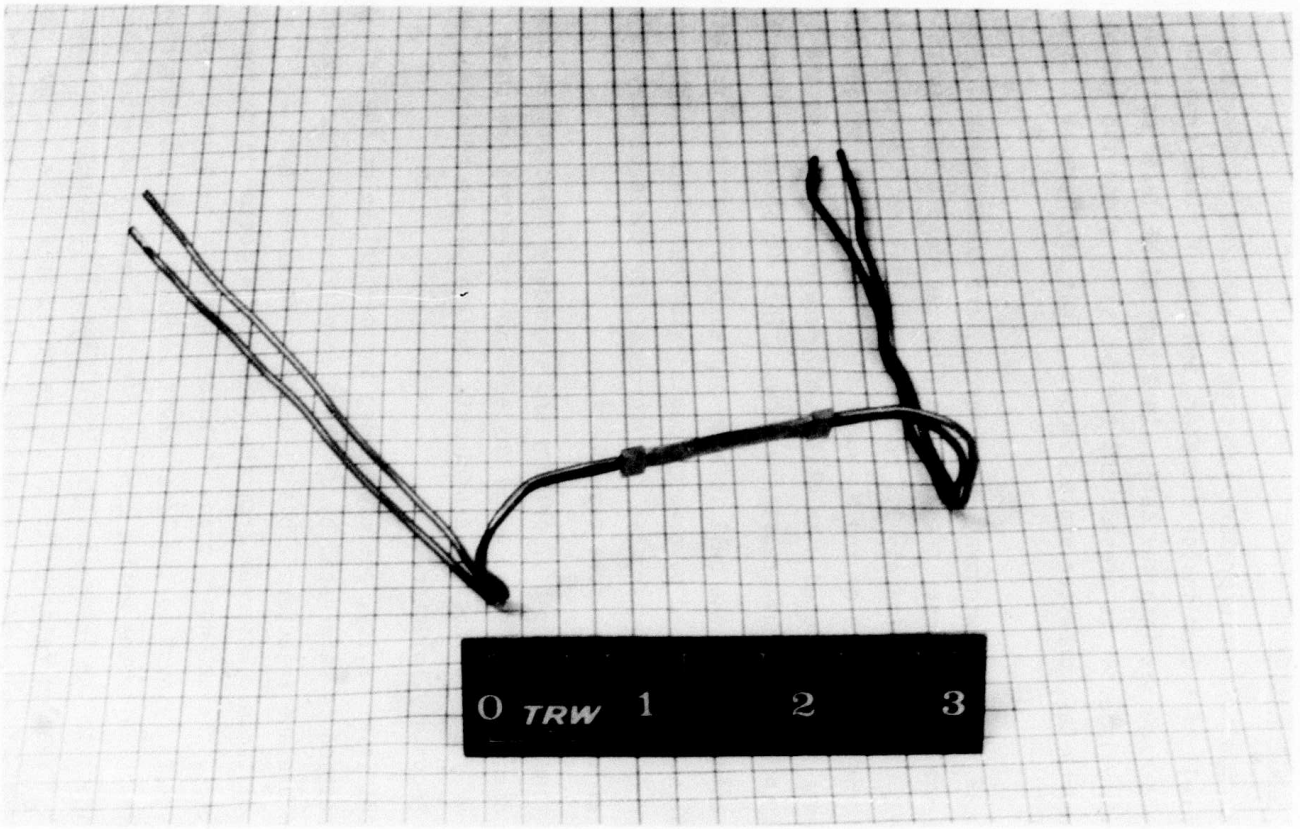

Figure 6. Water-Cooled Nickel Secondary Blade Injector. The Scale Is in Inches.

2.1.1.5 Laser Cavity

The combustor/nozzle/primary injector is attached to a water-cooled, aluminum cell of 5.0 cm inside diameter, and the HF flame from the primary injector is free jet into the cell. In a typical HF laser configuration, no secondary injector is present and the two sides along the lasing axis are closed by CaF_2 brewster angle windows. This arrangement is shown in Figure 7.

The CaF_2 brewster windows, when present, are purged with N_2. In a laser of these small dimensions, the N_2 purge flow can result in a substantial fraction of the approximately 1.7 torr cavity pressure. In order to avoid the arbitrary influence of the N_2 purge flow, the initial staged combustion experiments were completed with flat sapphire windows closing the sides of the cell in place of the brewster windows. This is shown in Figure 1.

The third side of the cell is also closed by a flat sapphire window. The final side is closed by a water cooled aluminum plate which provides the water cooled holder and gas feed throughs for the secondary injector as well as a cavity pressure tap location.

The final arrangement of primary and secondary injectors is shown in Figures 8 and 9. While two wedge shaped blade injectors are shown, for all the NF staged combustion experiments, only a single blade was used for the secondary injector.

In the laser cavity, position along the centerline of the cell in the flow direction is referenced by distance downstream from the aft end of the Busemann biplane injector. This distance is referred to as X_c. In a similar manner, distance downstream from the secondary injector is designated X_c'. In practice, the secondary blade injector is always held in the same position with respect to the laser cavity. However, a set of spacers are available to raise the entire combustor/nozzle/primary injector section with respect to the laser cavity. The difference between the origin of the X_c and X_c' axes is referred to as ΔX_c as noted in Figure 1. ΔX_c can change from a nominal value of 1.3 cm without any spacers to a maximum of 7.3 cm, progressing in 1 cm steps.

In the actual experimental set up, it was necessary to add a second cell downstream from the first cell since the NF emission extended for a

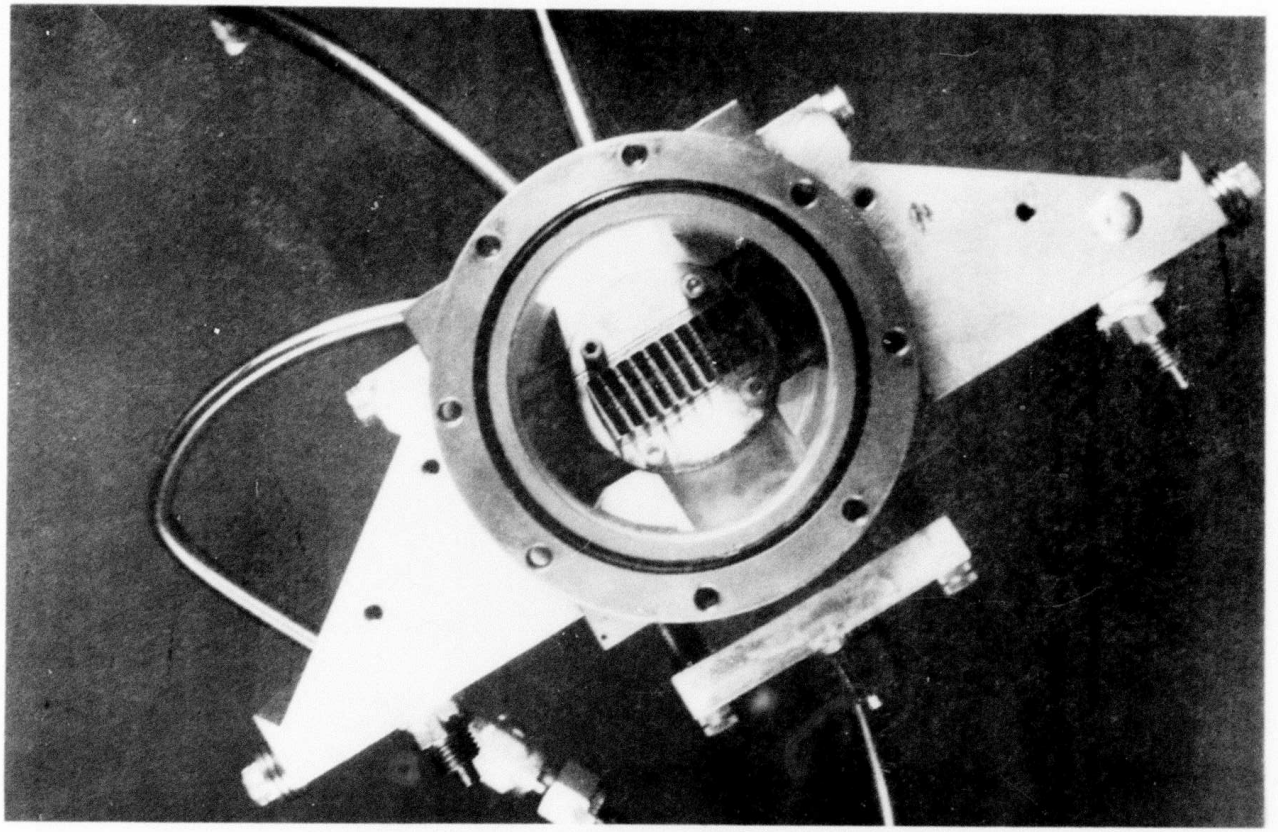

Figure 7. Upstream View of HF Laser Cavity Configuration Showing 9-Vane Injector and CaF_2 Brewster Window Holders Along Lasing Axis. No Secondary Mixer Is Present.

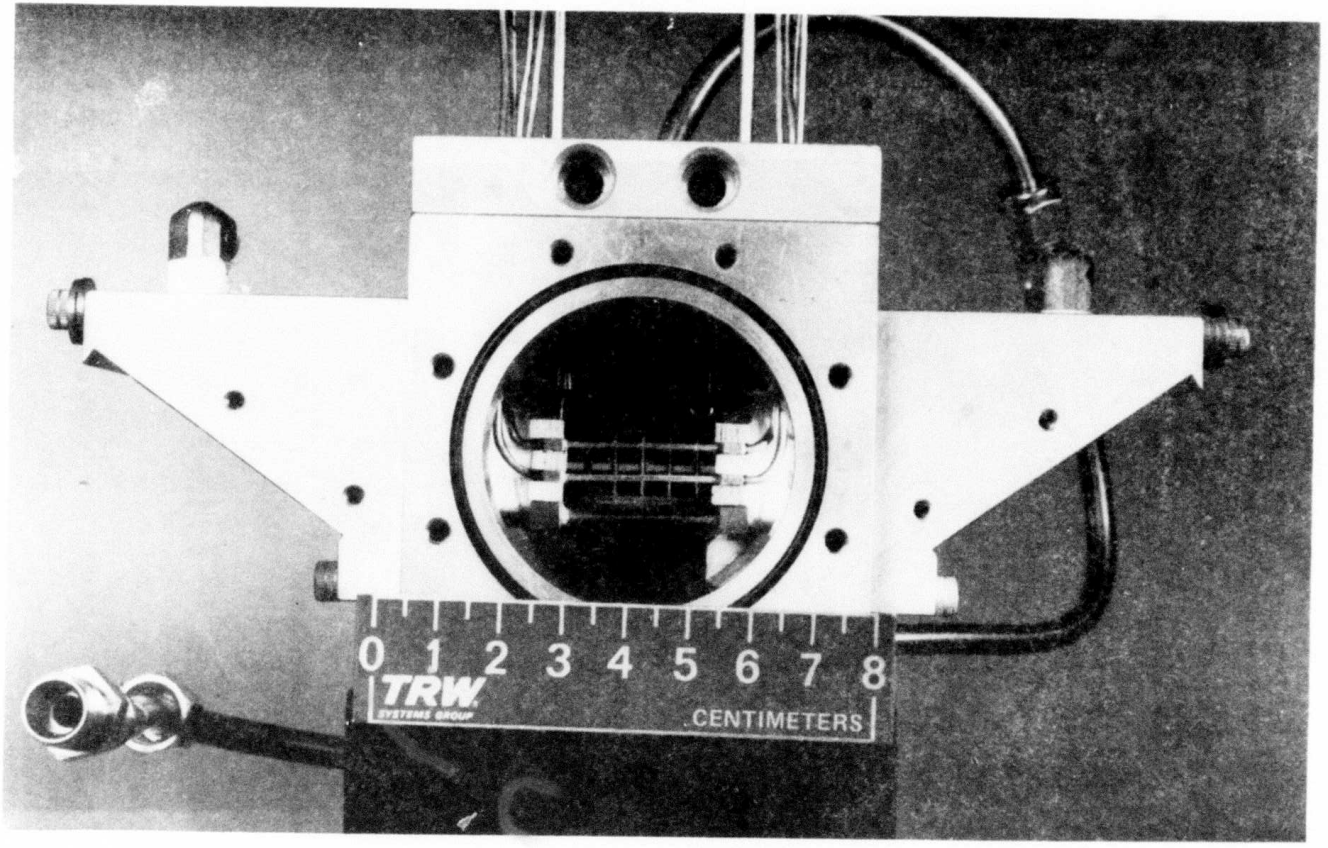

Figure 8. Upstream View of Staged Combustion Laser. The 5-Vane Primary Injector and Two Blade Secondary Injector Are Shown. Only a Single Blade Secondary Injector Was Used in the Present Experiments. The CaF_2 Brewster Window Holders Placed Along the Lasing Axis Are Also Shown.

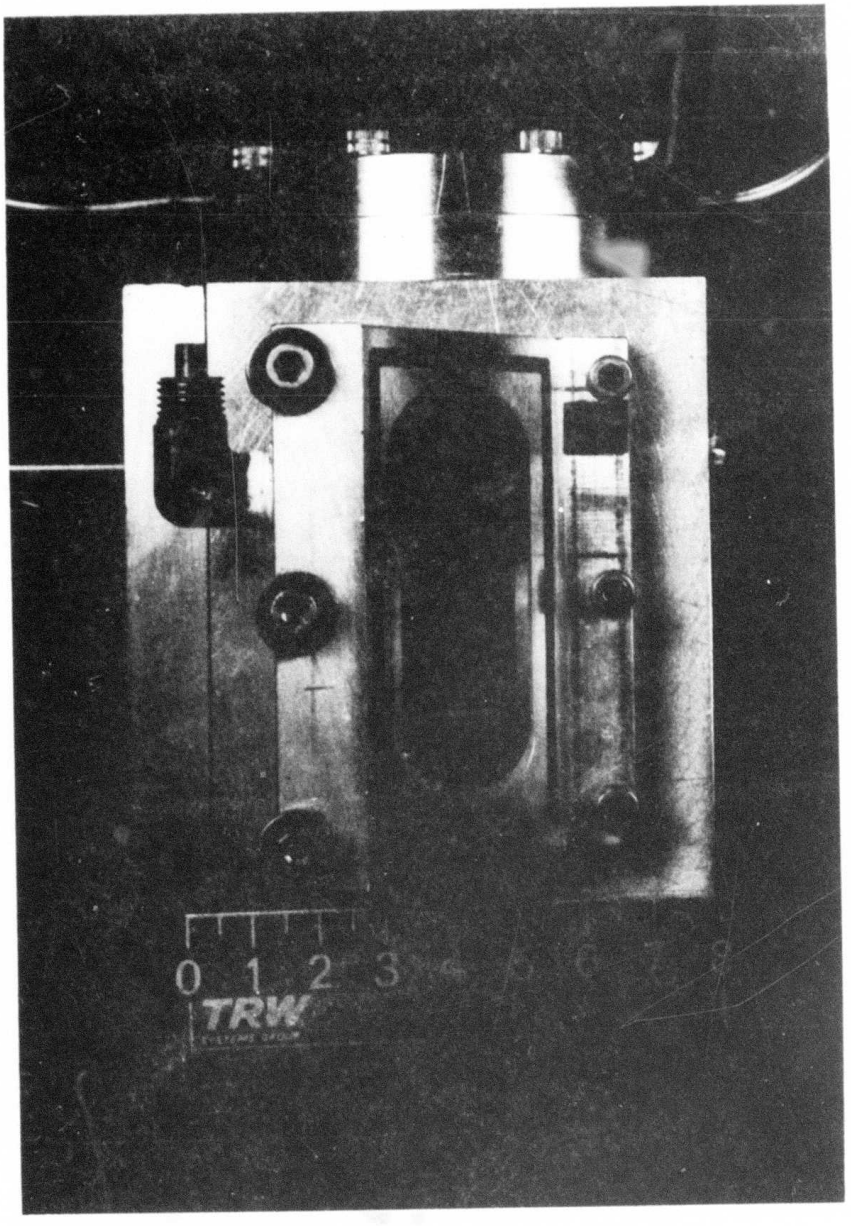

Figure 9. Side View Along Lasing Axis of Staged Combustion Laser. Gas Flow Is From Top to Bottom. The Fixture Holding Two Secondary Blade Injectors Is Visible Inside the Laser Cavity.

17

considerable distance. The final arrangement showing both cells is displayed in Figure 10. This second cavity is a nickel cell of 5.0 cm inside diameter. It is enclosed on three sides with flat sapphire windows. A pressure tap is located in the metal plate closing the fourth side. This pressure tap side corresponds to the same side the pressure tap is located in the first, or upstream cell.

In the final arrangement, the field of view of the flat sapphire windows in the upstream or No. 1 cell extends from X_c' = -2.1 cm to 4.0 cm. The pressure tap in this cell is designated P_1 and is located at X_c' = 2.1 cm. In the downstream or No. 2 cell, the viewing region extends from X_c' = 10.6 cm to 16.8 cm. The pressure tap in this cell is designated P_2 and is located at X_c' = 15.0 cm.

The cavity pressure at P_1 and P_2 was monitored by separate 0-10 torr MKS absolute capacitance manometers capable of $\pm$ 0.05 torr measurements. The combustor pressure P_c is monitored by a CEC strain guage type pressure transducer of 1 psia (51.7 torr) full scale sensitivity and is capable of $\pm$ .5 torr measurements.

The cavity gases pass through a water cooled heat exchanger and soda lime chemical trap prior to being pumped away by a large capacity Roots blower – fore pump vacuum system. The vacuum system is capable of 0.01 torr background pressures in the laser cavity and has an ultimate capacity in excess of 0.3 moles/sec or 3400 liters/sec at cavity pressures of about 1 torr.

2.1.2 Gas Delivery System

The combustor gases F_2 and D_2, and cavity gas H_2 are all metered to the laser by critical flow orifices contained in a flow control panel. As long as the pressure drop across the orifice is > 2, sonic flow is established through the orifice and gas flow is linearly proportional only to upstream gas pressure. The orifice upstream pressure for these gases is varied between 0.5 and 3 atm, and the various valves and metal tubing used in the gas lines are such that the > 2 pressure drop for sonic flow is easily maintained. The combustor operating pressure of about 30 torr and cavity pressures of several torr present no substantial back pressure, and even the small holes associated with the Busemann primary injector present no

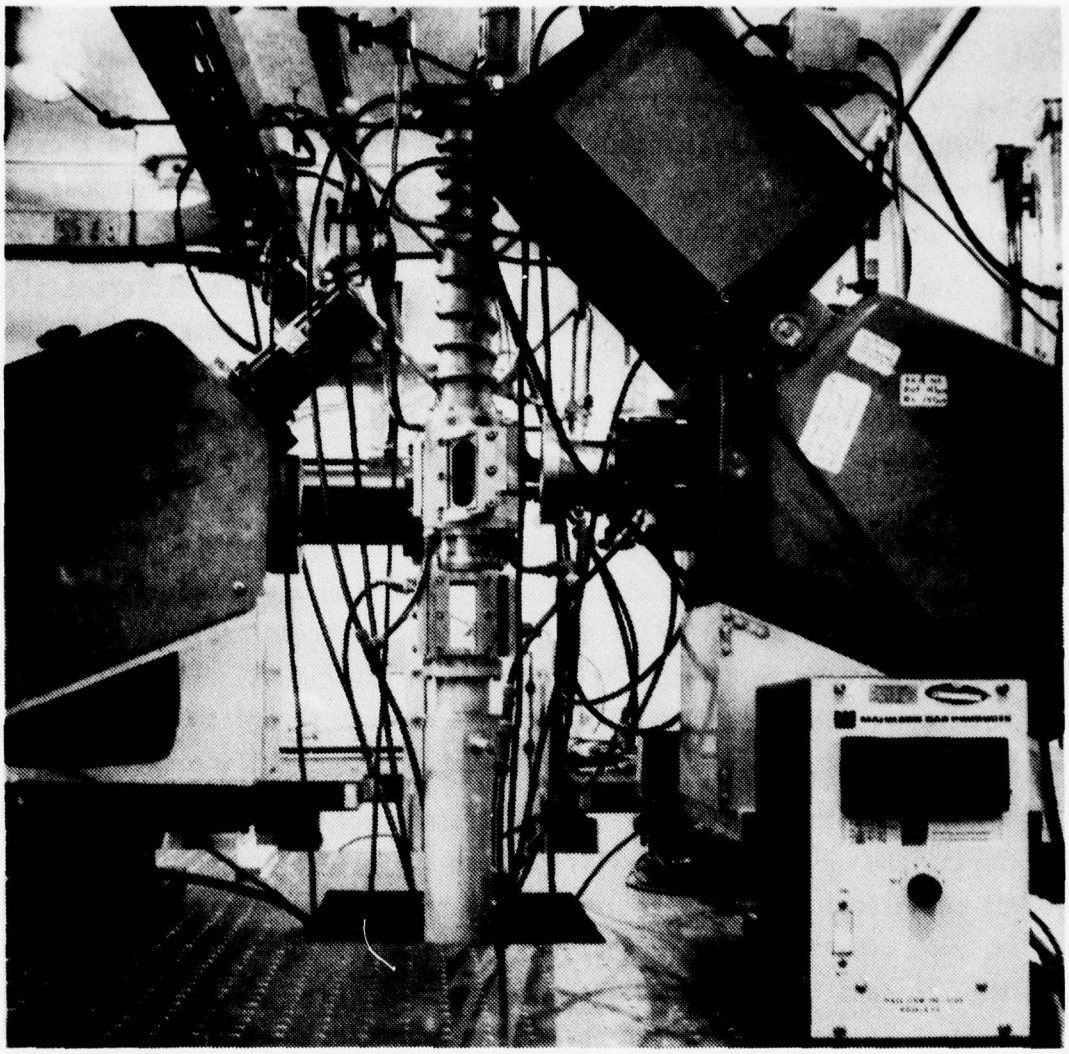

Figure 10. NF Staged Combustion Experimental Setup. The Gas Flow Is From Top to Bottom. On the Right Is the Spectrometer for Observation of HF Infrared Emission; on the Left Is the Visible Wavelength Spectrometer. The Toroidal Mirror Has Been Removed From the Infrared Spectrometer to Permit a Clearer View of the Laser Cavity.

appreciable pressure drop at the gas flows involved.

The combustor He flow is delivered by a glass rotometer device, and its delivery pressure is maintained at its calibration value of 10 psig by a regulator, insuring the validity of its flow calibration. On those occasions where N_2 purge gas is used for the brewster angle windows, a similar rotometer system is used.

The N_2F_4 delivered to the secondary blade presents a different situation. The high molecular weight of N_2F_4 and the small holes (ten, 0.01 cm diameter holes) associated with the blade injector make this the limiting sonic orifice in the gas line. At the flow rates involved for N_2F_4, the pressure immediately upstream from the blade orifices is about 0.5 to 1 atm pressure; the downstream pressure is several torr, i.e., the pressure of the cavity. However, the blade, while water cooled, is immersed in the HF flame from the primary injector and since mass flow through a sonic orifice is proportional to $T^{-\frac{1}{2}}$, the N_2F_4 flow at constant upstream pressure can vary as the blade heats up during the course of an experiment. Therefore, a Matheson linear mass flow transducer is used to record the N_2F_4 flow during an experiment rather than relying on any previous orifice calibration.

These Matheson linear mass flow transducers are also utilized to calibrate the critical flow orifice system and rotometers used for the balance of the gases. The flow transducers do not depend, over a wide range of values, upon the pressure and temperature of the gas flowing through it, but, in fact, they measure the amount of material flowing through utilizing a measured temperature rise in a slightly heated capillary tube. This allows the flow transducer to be conviently placed at some point within the actual flow system used in the experiment. The flow transducer has been previously calibrated with dry N_2 gas by the manufacturer, and this calibration is periodically verified by TRW Metrology.

If the flow transducer is used with another gas besides N_2 (e.g., He, H_2, D_2) a simple one-number correction factor is utilized which relates the change in specific heat capacity and density between N_2 and the test gas. Such a technique results in flow calibrations for the sonic orifices with about $\pm$ 5 percent accuracy.

In practice for expensive or toxic gases such as F_2, N_2F_4, etc., a dummy inert gas is used for the orifice calibration. This dummy gas flow calibration can be corrected to give a calibration for the experimental gas by using well established formulas for sonic flow. The ratio of the molar flow rate of two gases A and B for the same sonic orifice and upstream pressure and temperature is

$$\frac{\text{Flow A}}{\text{Flow B}} = \frac{K_A}{K_B}\sqrt{\frac{M_B}{M_A}} \tag{7}$$

where M_A is the molecular weight of gas A and

$$K_A = \gamma^{\frac{1}{2}}\left(\frac{2}{\gamma+1}\right)^{\left(\frac{\gamma+1}{2(\gamma-1)}\right)} \tag{8}$$

for γ equal to the ratio of heat capacity at constant pressure to the heat capacity at constant volume for gas A. This sonic orifice correction factor is different from that used to correct the flow transducer for different gases other than N_2.

The correction factor formula for the sonic flow orifices ignores small viscous effects present in the gas flow. To further account for these, a dummy gas of similar molecular weight and size to the experimental gas is used, e.g., Ar is used for F_2 calibrations. Since the N_2F_4 flow was being monitored directly during the course of an experiment by the flow transducer, a prior calibration with a dummy gas for N_2F_4 was not necessary. However, in some cases N_2F_4 was delivered to the primary Busemann injector and H_2 to the secondary injector. The size of the orifice in the Busemann injector is such that N_2F_4 could now be metered by a critical flow orifice in the flow control panel in the usual manner. (The only reason that the Matheson flow transducers are not used at all times for all gases is their cost. In general, they are used only to calibrate the critical flow orifice system.) In this case, SF_6 was used as a dummy calibration gas for N_2F_4.

In order to demonstrate the validity of these various correction factors, a calibration was done using N_2F_4 itself as the test gas as well as SF_6 (the flow transducers are all stainless steel construction, so the use

of N_2F_4 is permissible). Similar tests had been done previously comparing H_2, D_2 and the He flow through the same orifice with good results. However, the direct N_2F_4 calibration gave about 50 percent higher flow rate than the N_2F_4 calibration derived from SF_6. Repetition of the experiments (over several days time) gave good reproducibility for the results.

It was necessary then to check if the discrepancy lay in the flow transducer itself, the flow transducer correction factor, or the orifice flow correction factor. A system was put together which would allow a metered flow through a flow transducer to enter a known volume. The pressure rise associated with a measured time of flow results in a measurement of flow rate which utilizes only the ideal gas equation. No knowledge of heat capacities, molecular weight, or viscous effects is required.

As an example of this experiment, Table 1 shows the measurement for N_2 gas, which requires no correction factor for the flow transducer.

Table 1. N_2 Flow Rate x 10^{-5} Moles/Sec

Derived From Flow Transducer	Measured From Flow Into Known Volume Experiment	% Deviation
88	92	+ 4.5
54	57	+ 5.6
20	20	0

The results are in good agreement with the flow transducer.

Measurements that were done next used SF_6 and Ar as the test gases. Table 2 shows these results. The measurements using SF_6 and Ar require correction factors of 0.295 and 1.396 respectively to be applied to the flow transducer output, and these results represent the validity of applying such correction factors. In addition, the reproducibility of the results is shown since the first three SF_6 points were taken on a different day from the second three points.

Table 2. Test Gas Flow x 10^{-5} Moles/Sec

Test Gas	Derived From Flow Transducer	Measured From Flow Into Known Volume	% Deviation
SF_6	62	56	- 9.7
SF_6	32	29	- 9.4
SF_6	16	15	- 6.3
SF_6	16	15	- 6.3
SF_6	32	30	- 6.3
SF_6	62	56	- 9.7
Ar	78	85	+ 9.0
Ar	150	162	+ 8.0
N_2F_4	40	20	-50.0

Table 2 also shows the measurement for N_2F_4 itself. The flow derived from the flow transducer is a factor of two higher than the measured volume flow. This descrepancy is reproducible.

The measured volume experiment should represent the true molar flow rate for N_2F_4 as it does not rely on any correction factors. The flow transducer correction factor of 0.368 is based upon well established data for the heat capacity and molecular weight for N_2F_4 (JANAF) but apparently some error does exist. Table 3 shows how several representative flow transducer correction factors are calculated. For a flow transducer calibrated for N_2, the correction factor is multiplied by the apparent flow rate for N_2 to get the actual flow rate for the test gas.

Impurities in the N_2F_4 might be the cause of the error. However, two N_2F_4 bottles obtained about eight months apart gave the same results. Moreover, reasonable impurities such as N_2, NF_3 or F_2 would only increase the discrepancy since they have larger correction factors than N_2F_4.

Table 3. Flow Transducer Correction Factors

Test Gas	Specific Heat Capacity C_p at 21°C (cal/gr°K)	Density at 21°C, 1-Atm (g/liter)	ρC_p at 21°C (cal/liter°K)	Correction Factor $(\rho C_p)_{N_2} / (\rho C_p)_{gas}$
N_2	0.2485	1.1610	0.2885	1.000
F_2	0.1978	1.5750	0.3115	0.926
Ar	0.1246	1.6580	0.2066	1.396
NF_2	0.1885	2.156	0.4064	0.710
SF_6	0.1589	6.1410	0.9758	0.295
SiF_4	0.1681	4.3550	0.7321	0.394
N_2F_4	0.1819	4.3115	0.7843	0.368
$C_2Cl_2F_4$	0.1568	7.1220	1.1167	0.175

An N_2F_4 flow transducer correction factor of 0.185 would be required to provide agreement between the flow transducer and measure volume experiment. A correction factor of 0.185 is indicative of a high molecular weight, larger polyatomic molecule (see for example, $C_2Cl_2F_4$ in Table 3). The manufacturer's stated purity is 95 percent N_2F_4, and it is unlikely that there is a substantial variation from this since the gas acted in all other ways as N_2F_4. Even the presence of a substantial amount of NF_2 would not explain the discrepancy.

The conclusion from these results is that the flow transducer correction factor calculated in the usual manner for N_2F_4 is a factor of two too large. The measured volume experiments are straightforward and are believed to represent the true flow. This has been born out by the balance of the data in Tables 1 and 2. Therefore, a revised correction factor of 0.185 will be used for N_2F_4 whenever it is used directly with the flow transducer.

All reagent gases are used without further purification. The deuterium gas was supplied by the Government without a stated purity level; it is assumed to be technical grade. The manufacturer's stated purity is given in Table 4.

Table 4. Manufacturer's Stated Gas Purity

Gas	Manufacturer	Grade	Purity (%)
F_2	Air Products	Technical	97
He	Air Products	High Purity	99.995
H_2	Air Products	High Purity	99.9
N_2	Air Products	Ultra High Purity	99.998
D_2	U.S. Govt. Supply	Technical	98
N_2F_4	Hercules	—	95
NO	Matheson	C.P.	99

2.1.3 Optical Diagnostics

The optical diagnostics associated with these experiments consists of observation of emission in both the infrared and visible region. The infrared diagnostic covers the region 2.5 to 3.2 μm to observe the HF Δv=1 emission in order to determine HF(v) number density and gas temperature. The visible diagnostic covers the 500 to 900 nm region to observe the $NF(a^1\Delta)$ and $(b^1\Sigma^+)$ as well as $N_2(B^3\Pi_g) \rightarrow (A^3\Sigma_u^+)$ emission. Both wavelength regions were monitored with 0.3 m McPherson spectrometers.

2.1.3.1 Infrared Diagnostics

A liquid nitrogen cooled, InSb photovoltaic detector is used with a chopper and lock-in amplifier for phase sensitive detection. Spectra are displayed on a strip chart recorder. A 150 L/mm, 4 μm blaze grating in the 0.3 m spectrometer is used in first order for a dispersion of 21.22 nm/mm. For the HF spectral scan, a nominal slit width of 94 μm and therefore a resolution of about 2.0 nm is used, but in practice the FWHM for a well isolated HF line (e.g., $P_2(4)$) was determined experimentally for the actual slit opening in order to accurately determine the resolution. Care was taken that both entrance and exit slits of the spectrometer were open equally to insure a triangular slit function. Both an accurate resolution and triangular slit function are required for determination of absolute number densities. The slit height (i.e., length in the nondispersive direction) is 2 mm, and the spectrometer has been mounted on its side (Figure 10) so the slit height is horizontal and therefore perpendicular to the flow axis. This gives maximum spatial resolution of emission along the flow axis. A 2 μm long wavelength pass filter is used to block interfering second order spectra. The slit image is focused on the entrance slits of the spectrometer using a front surface, aluminized toroidal mirror. The toroidal mirror has a 10 cm focal length and 45° focusing half angle for a 1:1 magnification of the slit image.

The entire optical path and spectrometer is enclosed and flushed with dry nitrogen to remove the atmospheric water vapor which interfers with the HF spectrum. The optical system/detector is frequently calibrated with a 1000°K black body prior to any absolute intensity measurements. Care is taken to use a flat sapphire window or CaF_2 brewster window in the calibra-

tion depending upon what is used in the actual experiment. The HF spectra is distinct enough that the lines are readily identified and provide their own wavelength calibration.[10]

The peak intensity of the HF lines are hand read and input to the CHEMLUM computer code[11] along with the calibration data. The code constructs Boltzmann plots, Ln(I/F) versus E(v,J) where I is the absolute line intensity, F is a statistical and line strength weighting factor, and E(v,J) is the energy for vibration-rotation state (v,J) from which the emission originates. The code computes the rotational temperature (assumed to be equal to the local gas temperature), vibrational number densities, and line-by-line gains of the excited species. HF(1 → 0) emission data is ignored in the rotational temperature determination due to usually non-linear Boltzmann plots resulting from self absorption by ground state HF. Measurements are taken along what is usually the lasing axis of the HF laser, and, therefore, the depth of the optical signal is taken to be 3.5 cm, slightly larger than the nozzle length 3.1 cm, to account for expansion in this direction.

2.1.3.2 Visible Diagnostics

The visible diagnostic extends from 500 nm to 900 nm in the near infrared. A GaAs photomultiplier tube (RCA C31034A) covers this entire range. The PMT is used at 1500 V operating voltage with a picoammeter to measure the anode current. The output is displayed on a strip chart recorder. A 600 L/mm, 750 nm blaze grating in the 0.3 m spectrometer is used in first order for a dispersion of 5.31 nm/mm. A nominal slit width of 95 μm is used for a resolution of 0.5 nm, but again a convenient narrow emission source such as a He-Ne laser or HF Δv=3 vibration-rotation lines which fall into this spectral region is used to determine the actual resolution. Care is taken to insure that both slits are the same width to give a triangular slit function. This is especially important for quantitative NF spectral measurements since the vibration-rotation structure of the electronic spectra is somewhat broader than the slit width. A triangular slit function of known resolutions makes deconvolution of the observed spectra straightforward. The slit height is 2 mm, and with the spectrometer on its side , the slit is oriented in a horizontal manner, perpendicular to the flow axis (Figure 10). A 4800 Å long wavelength pass filter is used for

order sorting. As in the infrared case, a 1:1 magnification, 10 cm focal length, 45° half focus angle front surface aluminized mirror is used to image the emission light on the entrance slit.

In some of the initial measurements made under this program for $NF(b^1\Sigma^+)$ emission, inadvertantly an entrance slit of 190 μm and an exit lsit of 270 μm was used. The resolution here is 1.4 nm, but this configuration has a trapozoidal slit function. No absolute data was taken at this setting and there is no problem in comparing relative data all taken at this same slit setting.

The sensitivity calibration prior to an absolute measurement is done using an Epply ribbon filament lamp with an absolute calibration traceable to NBS. Again, a flat sapphire or CaF_2 brewster window is included in the calibration depending upon what is used in the actual experiment. The wavelength calibration near the 880 nm region is supplied by P and R branch lines of the $HF(3 \rightarrow 0)$ transition[10] observable in the HF flame. The $NF(b^1\Sigma^+)$ emission is a strong band with a distinctive head[12] and provides the wavelength calibration in the 530 nm region.

As mentioned above, both the infrared and visible spectrometer are placed on their sides to give a horizontal slit orientation with respect to the vertical gas flow. An important experimental parameter is the observation of the emission signals as a function of distance X_c' along the flow axis (see Figure 1). In general, both spectrometers view the staged combustion reaction cell along the lasing axis, with each spectrometer positioned at opposite sides of the reaction cell. The gas depth for both is taken as 3.5 cm to account for the slight gas expansion in this direction from the 3.1 cm nozzle length. Care is taken to insure that both spectrometers are viewing the center of the reaction cell and are at the same value of X_c'. The entire staged combustion laser apparatus can be vertically translated with respect to these spectrometers by means of a flexible bellows attached to the pumping line. The bellows system holds the staged combustion apparatus rigid at any one position, but by moving the reaction cell, the spectrometers can view the cell at different X_c' values. The position of the spectrometers is such that they view the same X_c' region simultaneously.

A polaroid portriature camera was used to photograph the flame from

the reaction cell. This is found to be a more reliable measure of the shape and homogeneity of flame than visual observation. However, the polaroid film seems to be most sensitive to the yellow-colored flame resulting from N_2 first positive emission, and in this way is not a direct measure of the NF emission. On those occasions where the NF($b^1\Sigma^+$) emission dominated and the flame was indeed a bright green, the polaroid film would reproduce the flame features.

2.2 RESULTS

A typical visible emission spectra is shown in Figure 11. The $\Delta v=5$ to $\Delta v=1$ vibrational progression of the $N_2(B^3\Pi_g) \rightarrow (A^3\Sigma_u^+)$ band dominates the spectra. The NF($b^1\Sigma^+$) emission at 529 nm is clearly visible. However, the region of NF($a^1\Delta$) emission is obscured by the $\Delta v=1$ N_2 first positive and HF($v=3 \rightarrow 0$) bands. When the flow of N_2F_4 being mixed into the HF flame is increased, the NF and N_2 intensities increase with respect to the HF($3 \rightarrow 0$). However, even when D_2 replaces the H_2 cavity fuel so as to eliminate the HF overtone signal, the NF($a^1\Delta$) signal is still obscured solely by the N_2 first positive $\Delta v=1$ band as shown in Figure 12. While D-atoms are as efficient a source to produce NF($a^1\Delta$) as H-atoms, Figure 12 does show the effect that the NF($b^1\Sigma^+$) intensity is greatly reduced with the use of D_2. For the same conditions in Figure 12 but with H_2 cavity fuel, the NF($b^1\Sigma^+$) would be off-scale by about a factor of two.

This difficulty in readily observing the NF($a^1\Delta$) state resulted in the initial set of experiments where only the NF($b^1\Sigma^+$) state was monitored as a function of gas conditions, staged combustion hardware configuration, and X_c'. The approach here was to find a set of conditions which maximized the NF($b^1\Sigma^+$) population density, and this might also be a region where the NF($a^1\Delta$) population density increased so to be observed more clearly from the interfering spectra.

2.2.1 N_2F_4 Primary Injector/H_2 Secondary Injector Experiments

The first staged combustion experiments involved mixing of N_2F_4 into the gas flow by means of the nine-vane primary Busemann biplane injector and H_2 being added downstream by a single blade secondary wedge injector. This configuration permitted observation of the maximum NF(b) signal within the viewing region of the first, upstream cell. This minimizes the trans-

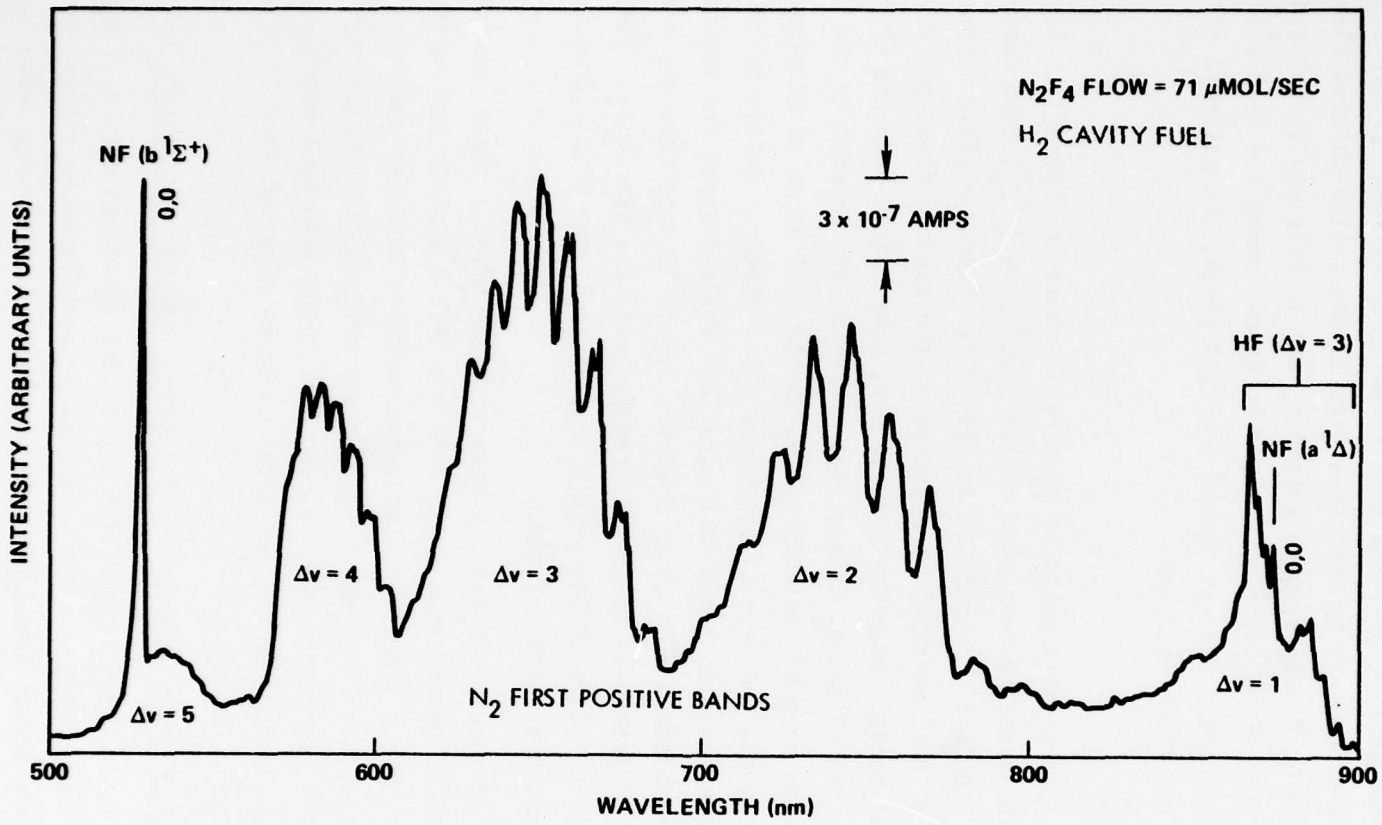

Figure 11. Typical Visible Region Spectra for NF System Using H_2 Cavity Fuel. The Spectral Resolution Is 1.4 nm.

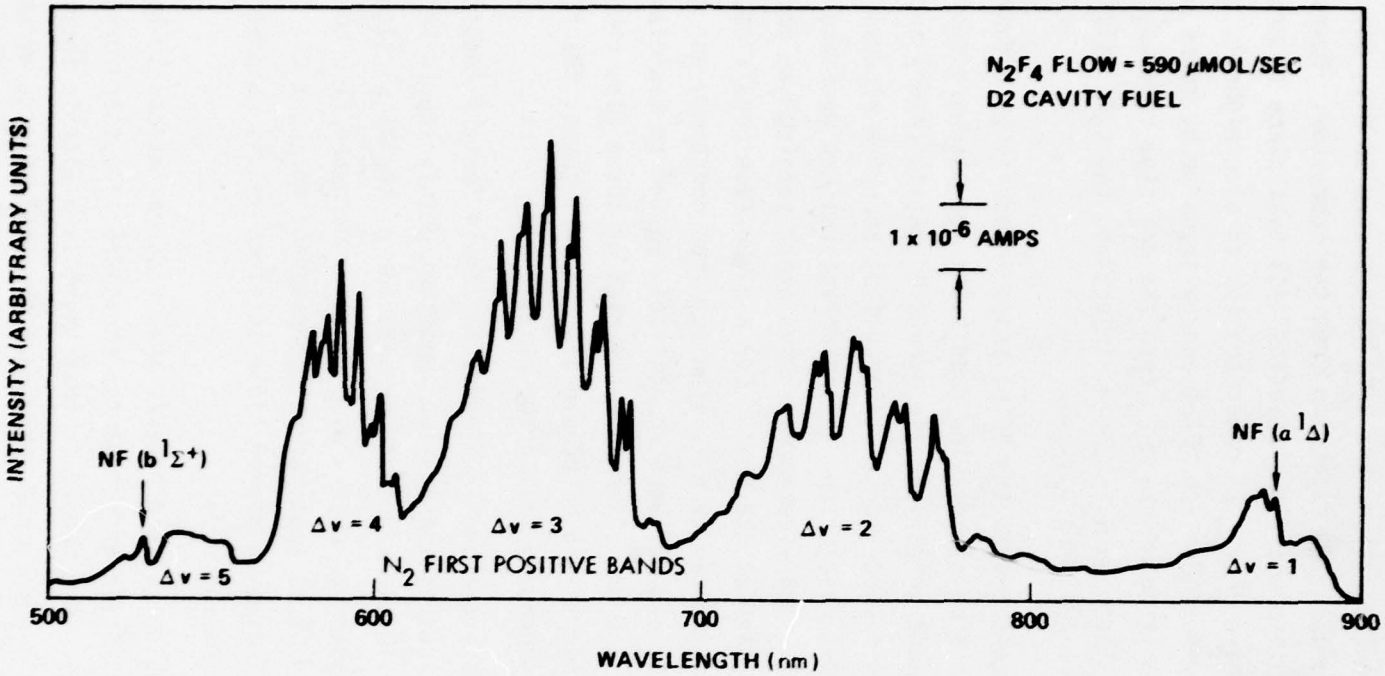

Figure 12. Typical Visible Region Spectra for NF System Using D_2 Cavity Fuel. The Spectral Resolution Is 1.4 nm.

lation of the spectrometers required to scan the entire X_c' region of interest.

For this configuration, the N_2F_4 is expected to mix, but not react, with the F/DF/He gas flow expanding from the combustor. Downstream where the H_2 is mixed into the flow, reaction will take place to produce NF(a) in the region where HF($v \geq 2$) concentration is also highest, thus giving good opportunity for NF(a) to NF(b) energy transfer by means of HF($v \geq 2$). In addition, if mixing of the N_2F_4 into the gas flow is slow, by increasing the distance ΔX_c between N_2F_4 and H_2 injection, the N_2F_4 will have more time to fully mix prior to reaction.

For these experiments the NF(b) state intensity as a function of X_c' was observed for a matrix of flow conditions and hardware configurations including different primary nozzle expansion ratios (A/A*) and varying ΔX_c values. These experiments utilized flat sapphire windows on the cavity and 1.4 nm optical resolution. All observations are made along the lasing axis of the cell. The spectrometer wavelength setting was position for maximum NF(b) signal at 528.8 nm. For a given flow condition, the value of the combustor F_2 and cavity N_2F_4 flow remained constant, and the balance of the gases, He, D_2 and H_2, were repetitively varied to maximize the NF(b) signal at X_c' = 3.0 cm. Then X_c was varied at these flow conditions to observe the change in the NF(b) signal. For all cases, the flame appeared yellow and homogeneously filled the reaction cell.

The results are shown in Figures 13 and 14 for the conditions given in Tables 5 and 6, respectively. Two important points should be noted. First, no major change in the magnitude or behavior of the NF(b) signal as a function of X_c' is observed over a wide range of hardware/flow conditions. The maximum observed NF(b) state signal corresponds to about 2×10^{12} molec/cm^3. Second, for all cases, a reproducible local maxima is observed for NF(b) between 1 and 2 cm for X_c'.

The conclusion reached here is that wide variations in hardware/flow conditions have little effect on the chemistry and, therefore, the concentration of NF(b). One theory is that there is a kinetic bottleneck early in the reaction sequence and subsequent physical effects which would be expected to influence the chemistry are unimportant. The observed local

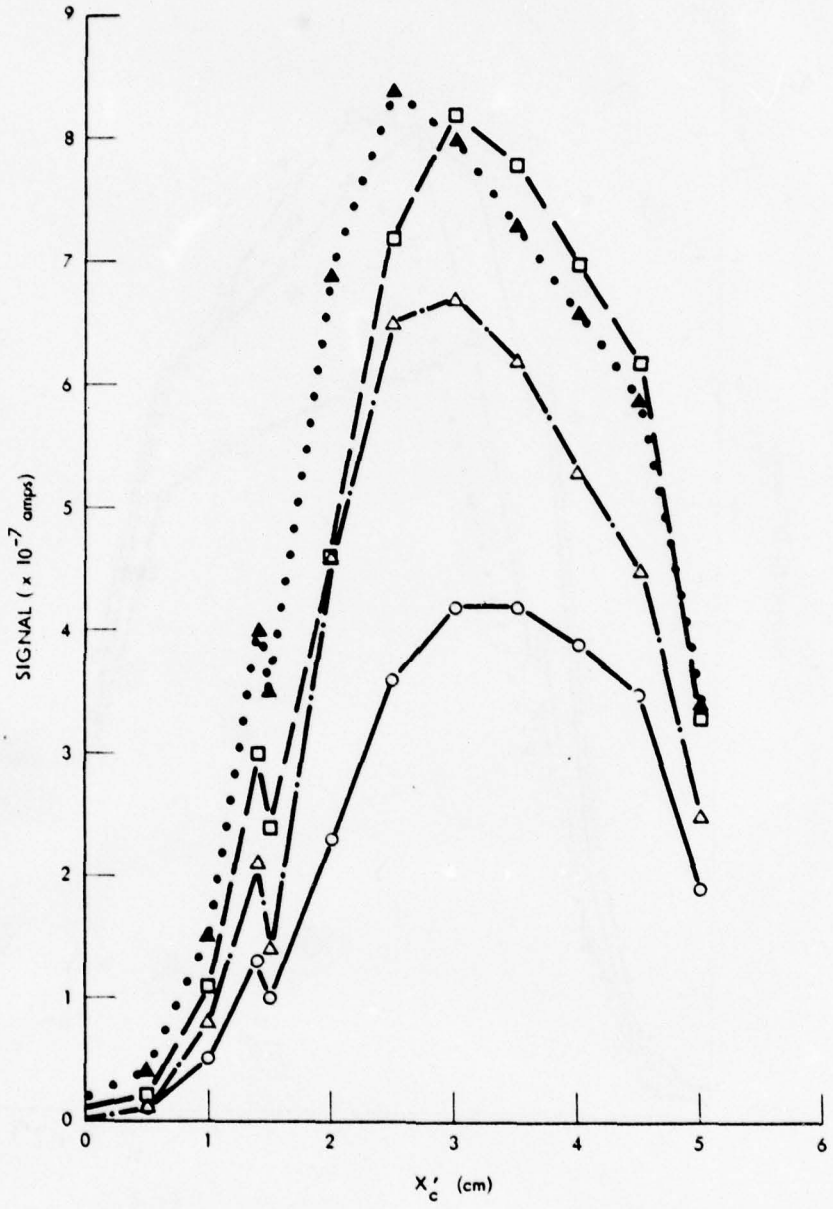

Figure 13. $NF(b^1\Sigma^+)$ State Intensity Versus X_c' for Case of N_2F_4 in Primary Busemann Injector and H_2 in Secondary Wedge Injector. Experimental Conditions Given in Table 5.

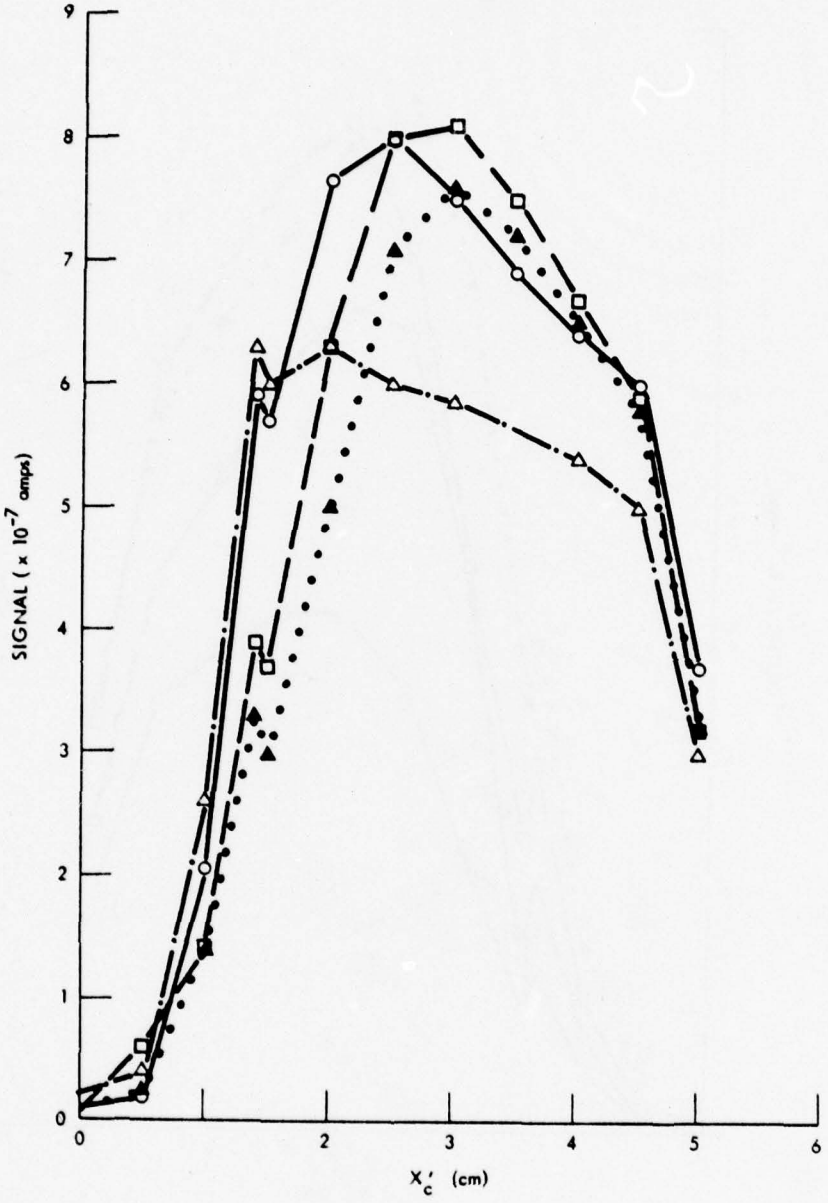

Figure 14. NF($b^1\Sigma^+$) State Intensity Versus X_c' for Case of N_2F_4 in Primary Busemann Injector and H_2 in Secondary Wedge Injector. Experimental Conditions Given in Table 6.

Table 5. NF Excited State Production Experimental Conditions.

CASE NO.	GAS FLOWS (10^{-3} mol/sec)					Pressure (torr)		Nozzle	
	Combustor			Primary	Secondary				
	F_2	D_2	He	N_2F_4	H_2	Combustor	Cavity	A/A*	ΔX_c (cm)
○ 1	3.0	1.4	3.0	0.4	1.5	19.5	1.58	10:1	1.3
△ 2	3.0	1.4	3.0	0.6	1.8	19.1	1.83	10:1	1.3
□ 3	2.0	0.9	3.0	0.6	1.7	12.6	1.48	10:1	1.3
▲ 4	1.0	0.5	0	0.6	1.3	5.2	0.94	10:1	1.3

Table 6. NF Excited State Production Experimental Conditions.

CASE NO.	GAS FLOWS (10^{-3} mol/sec) Combustor F_2	Combustor D_2	Combustor He	Primary N_2F_4	Secondary H_2	Pressure (torr) Combustor	Pressure (torr) Cavity	Nozzle A/A*	ΔX_c (cm)
○ 5	1.0	0.6	0	0.6	1.7	5.4	0.88	10:1	4.3
▲ 7	2.0	1.0	3.0	0.6	1.6	6.5	1.43	4:1	7.3
△ 9	1.0	0.7	0	0.6	1.6	3.0	0.91	4:1	7.3
□ 10	2.0	1.0	3.0	0.6	1.5	18.6	1.43	14:1	7.3

maxima may represent the reaction of NF_2 residual in the N_2F_4 prior to substantial heating. The ratio of this local maxima to the true maximum NF(b) signal may indicate that only a small amount of NF_2 is available. It is unlikely that the other reactants, H-atoms and HF($v \geq 2$), are not present in reasonable amounts. A similar local maxima was observed for some cases in LAMP code modeling of the NF system done at AFWL and it was associated with reaction of residual NF_2 prior to reaction of additional NF_2 produced by N_2F_4 thermal dissociation.[13]

The NF(a) state emission was also observed in these experiments. The intensity of the $N_2(B \rightarrow A)$ transition is strong, however, and interferes with a quantitative determination of NF(a) signal intensity.

Methane was used in place of the cavity H_2 in order to try and quantitatively observe NF(a). Methane can be used in the NF system because both

$$F + CH_4 \rightarrow HF(v) + CH_3 \tag{9}$$

and

$$CH_3 + NF_2 \rightarrow CH_3F + NF(a^1\Delta) \tag{10}$$

can take place.[2] While the NF(b) intensity is somewhat reduced ($\sim$ 3X) for CH_4 compared to H_2, the CH_4 still produces NF(a) and the yellow N_2 first positive emission is eliminated. This is because in contrast to reaction (5), the reaction

$$CH_3 + NF(a^1\Delta) \rightarrow CH_3F + N^*(^2D) \tag{11}$$

does <u>not</u> have sufficient exothermicity to produce the excited nitrogen atoms. However, while it is experimentally observed that the N_2 emission disappears, it is replaced by the rich electronic spectrum of the $CH_2(b^1B_1) \rightarrow (a^1A_1)$ band which also interferes with quantitative observation of NF(a).

2.2.2 <u>H_2 Primary Injector/N_2F_4 Secondary Injector</u>

These next experiments were identical to the previous ones described in Section 2.2.1 except now the H_2 cavity fuel is mixed upstream by the

nine-vane Busemann primary injector, and the N_2F_4 is added downstream by the single blade secondary wedge injector. This should allow the N_2F_4 to be mixed into a region of high temperature in the HF flame which may accelerate the thermal decomposition of N_2F_4. The NF(b) intensity is now observed to extend over the viewing region of both cells, and a point at $X_c' = 11.5$ cm in the downstream cell is picked to maximize the NF(b) intensity as a function of gas flow. Again, for a given flow condition, the value of the combustor F_2 and cavity N_2F_4 flow remain constant while the balance of the gases are repetitively varied.

For all these cases, the flame appeared yellow and originated as a triangular shaped free jet expansion from the secondary blade when viewed along the lasing axis. The yellow flame was not attached to the secondary blade and stood off about 0.5 cm in the downstream direction. By the time the flame reached the downstream cell it homogeneously filled the observation region.

The results are shown in Figure 15 for the conditions given in Table 7. P_1 and P_2 are the cavity pressure taps located at $X_c' = 2.1$ cm and 15.0 cm, respectively. Little variation in the NF(b) signal is observed for different flow conditions in the downstream region. For this reason, only Case 23 was studied in the upstream cell region. The maximum in the NF(b) signal apparently is in the region between the two cells which is not available for observation. However, from the intensity of the yellow flame and the trend in the data in Figure 15, the maximum NF(b) signal is expected to be about 1×10^{-8} amps.

The magnitude and insensitivity to gas flow conditions for the NF(b) signal is very similar to that observed in the experiments from Section 2.2.1 (Figure 13 and 14), and even a similar local maxima in NF(b) intensity is observed at $X_c' \cong 1.0$ cm. However, the maximum NF(b) signal is shifted downstream to about $X_c' = 9$ cm.

Case 25 in Figure 15 has the same F_2 and N_2F_4 flow as Case 23. For Case 25, $X_c' = 14.0$ cm was picked for the flow maximation of NF(b) intensity by the balance of the gases, D_2, He and H_2. The similarity between the flows and NF(b) signal for Cases 23 and 25 show that the choice of the X_c' value for initial flow maximation is not of major concern.

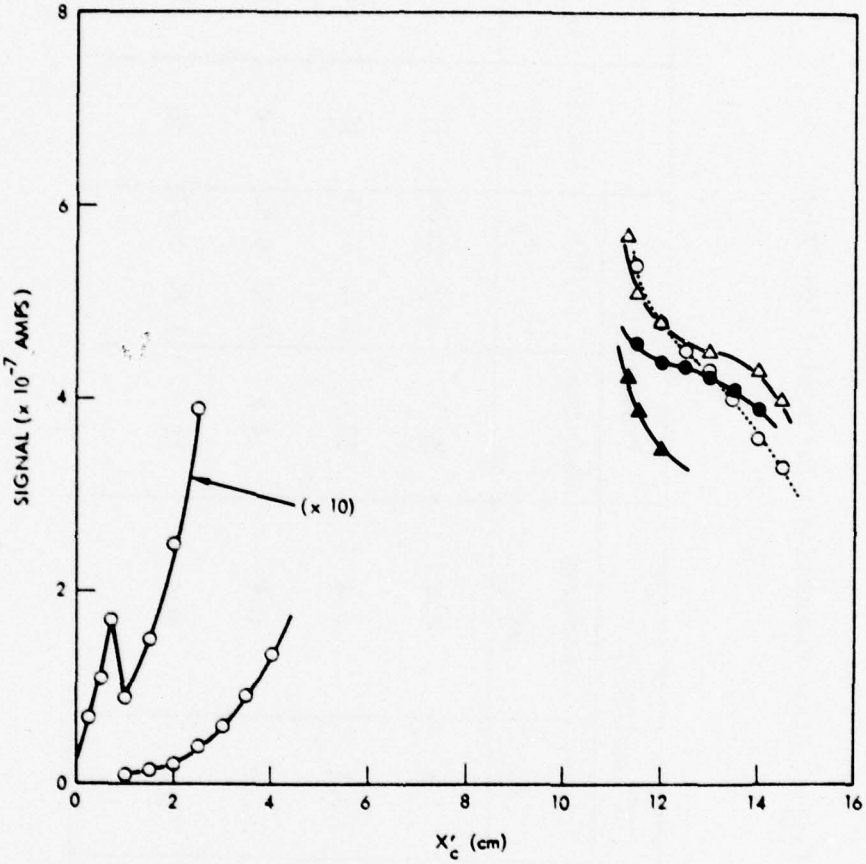

Figure 15. $NF(b^1\Sigma^+)$ State Intensity Versus X_c' for Case of H_2 in Primary Busemann Injector and N_2F_4 in Secondary Wedge Injector. Experimental Conditions Given in Table 7.

Table 7. NF Excited State Production Experimental Conditions.

Case No.	Gas Flows (10^{-3} mol/sec)					Pressure (torr)			Nozzle	ΔX_c (cm)
	Combustor			Primary	Secondary	Combustor	Cavity		A/A*	
	F_2	D_2	He	H_2	N_2F_4		P_1	P_2		
● 22	3.0	0.9	7.0	3.4	0.4	22.1	2.37	2.26	10	1.3
○ 23	2.0	1.3	7.0	3.3	0.4	20.1	1.72	1.73	10	1.3
▲ 24	1.0	0.5	0	2.9	0.4	4.7	0.92	0.93	10	1.3
△ 25	2.0	1.0	7.0	2.6	0.4	19.5	1.74	1.71	10	1.3

Again an attempt was made to observe NF(a) for the gas conditions and configuration of these experiments. The NF(a) is still obscured by the $N_2(B \rightarrow A)$ emission. It was found, however, that by reducing the combustor D_2 flow to 0.9 mmol/sec for Case 23, it was possible to change the flame to a bright green color. Presumably, reducing combustor D_2 reduces the free fluorine atoms available, and, thereby, reducing the H-atoms in the cavity. Without excess H-atoms, reaction (12)

$$H + NF_2 \rightarrow HF + NF(a^1\Delta) \tag{12}$$

can compete with reactions (13) and (14)

$$H + NF(a^1\Delta) \rightarrow HF + N^*(^2D) \tag{13}$$

$$N^*(^2D) + NF(a^1\Delta) \rightarrow N_2(B^3\Pi_g) + F \tag{14}$$

to eliminate the N_2 first positive emission. However, decreased H-atoms means there is less $HF(v \geq 2)$ to pump the $NF(b^1\Sigma^+)$ state. This is observed for the green flame case, for while the flame is green, indicative of $NF(b^1\Sigma^+)$ emission, the magnitude of the NF(b) signal is down about a factor of ten from the yellow flame conditions.

The NF(a) signal is also reduced due to decreased H-atoms flow, and the spectra is still obscured by the $HF(3 \rightarrow 0)$ overtone emission in the green flame. When H_2 is replaced by D_2 cavity fuel, the green flame turns pale yellow and it is finally possible to clearly observe the NF(a) state spectra at 874 nm. However, these are not optimum conditions to produce NF(a) and the signal is very weak.

2.2.3 Addition of Nitric Oxide to the Staged Combustion Device

As indicated in Section 2.2.2, it was possible to observe NF(a) emission but only for gas conditions which do not maximize the concentrations of NF(b) and NF(a). It is not possible to maximize the NF(a) signal at 874.2 nm because of the interference of the N_2 first positive signal. To circumvent this difficulty, nitric oxide at flow rates about 1×10^{-3} mol/sec is mixed in with the hydrogen cavity fuel leading to the Busemann primary injector. The NO is expected to remove the $N(^2D)$ atoms which are the precursor of

$N_2(B^3\pi_g)$ without substantially affecting the concentration of other gas species.[7] The NO flow is metered by a sonic flow orifice system similar to that used for the other gases (see Section 2.1.2), and it is mixed with the H_2 flow sufficiently far upstream to allow for mixing of the two gases prior to reaching the primary injector.

The major effect of NO addition is that the flame changes from yellow to bright green. Spectral scans of the visible region indicate that the N_2 first positive is almost completely absent, and the NF(a) spectra is clearly observed. Even the NF(b) $\Delta v = -1$ emission at 562 nm is clearly visible. If gas conditions are chosen which first maximize the NF(b) signal, upon addition of NO, the NF(a) spectra is about a factor of ten stronger than even the HF($3 \rightarrow 0$) spectra in the same region. It is not necessary to change to D_2 cavity fuel to clearly observe the NF(a) spectra.

It is now possible to adjust the gases to maximize the NF(a) signal. Case 27, given in Table 8, is a representative example. The F_2, N_2F_4 and NO flows remained constant while the balance of the flows are varied to maximized NF(a) at the $X_c' = 2.0$ cm position. The various gases could be adjusted over a fairly wide range without the return of the yellow flame supplanting the green flame. As long as the green NF(b) flame is observed in the reaction cell, the NF(a) signal is not interferred with. This fact is routinely checked by scanning the region of the NF(a) spectra. Figure 16 shows the quenching of the N_2 first positive signal at 650 nm in the region of the $\Delta v = 3$ progression.

The gas conditions which maximized NF(a) signal also are nearly the same which miximize NF(b). Figure 17 shows the NF(b) intensity as a function of X_c' for Case 27. During the course of experiments for Case 27, the available N_2F_4 supply was low, and decreased flow rates of N_2F_4 were necessary compared to Cases 22 to 25 given in Table 7. However, the magnitude and form of the NF(b) signal is about the same when comparing Figures 15 and 17.

Figure 17 also shows that NO has little effect on the NF(b) signal. The green flame has much the same shape and character as the yellow flame.

The NF(a) signal at 874.2 nm displayed in Figure 17 is similar to NF(b) in its X_c' dependence. The fact that both NF(a) and NF(b) continue

Table 8. NF Excited State Production Experimental Conditions.

Case No.	Gas Flows (10^{-3} mol/sec)							Pressure (torr)		Nozzle	ΔX_c (cm)
	Combustor			Primary		Secondary	Purge	Combustor	Cavity		
	F_2	D_2	He	H_2	NO	N_2F_4	N_2		P_1	A/A*	
27	2.0	0.9	8.6	0.8	1.1	0.25	0	19.8	1.25	10	1.3
38	2.7	1.7	5.5	1.8	2.2	0.49	31	21.8	6.07	10	1.3

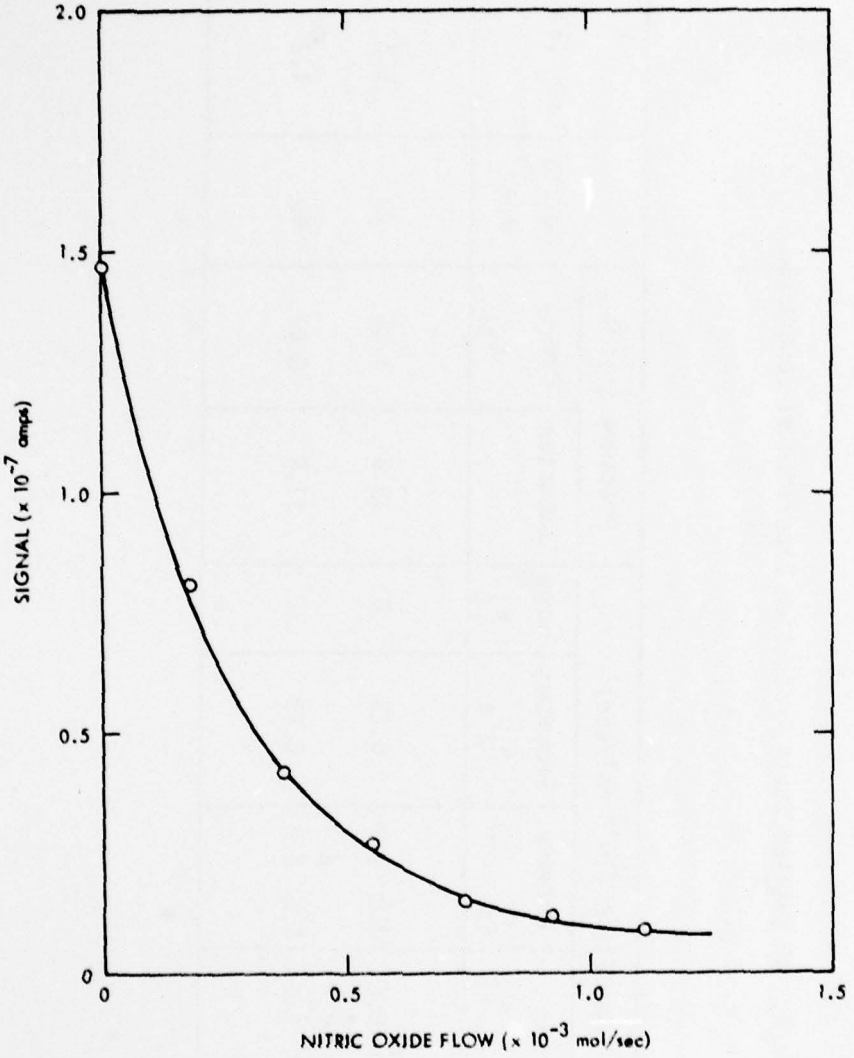

Figure 16. Variation of N_2 First Positive Signal in $\Delta v = 3$ Progression at 650 nm Versus Added Nitric Oxide Flow. The Spectral Resolution Is 1.4 nm and the Gas Conditions Are for Case 27 Given in Table 8. $X_c' = 2.0$ cm.

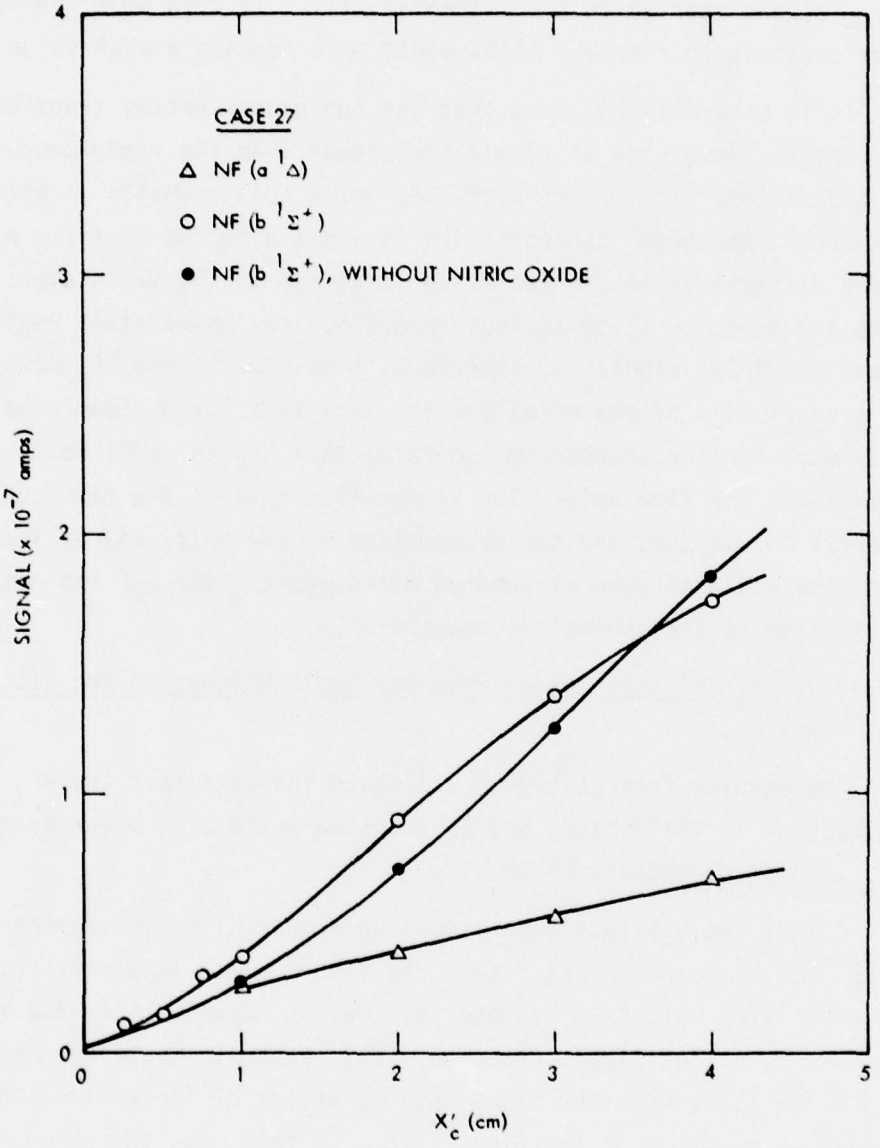

Figure 17. NF($a^1\Delta$) and ($b^1\Sigma^+$) State Intensity Versus X'_c for Case of H_2 and NO in Primary Busemann Injector and N_2F_4 in Secondary Wedge Injector. Experimental Conditions for Case 27 Given in Table 8.

to rise within the viewing region means the conversion of NF(a) to NF(b) by V-E energy transfer involving HF($v \geq 2$) has not reached a region where HF($v \geq 2$) has started to drop significantly. If this were the case, NF(a) might continue to rise but NF(b) would have reached a peak value.

It is generally believed that the subsequent energy transfer and quenching reaction involving NF(a) will be slower than its rapid production from NF_2 and H-atoms.[2,7] (In Figure 16, while the intensity of NF(a) is less than NF(b), the NF(a) concentration is about a factor of fifty higher due to the differences in the radiative lifetimes of the two states.) Hydrogen atoms are expected to be copious throughout the observation region of Figure 17 and the NF(a) signal is, therefore, a measure of the NF_2 concentration. The gradual rise of the NF(a) and the fact that its maximum signal is probably much farther downstream indicates that NF_2 is continually being produced along the flow axis. The linear flow rate of the gases corresponds to about 25 μsec/cm, and the observation of the NF(a) signal indicates that on a time scale of several hundred microseconds, the N_2F has not reached equilibrium in its thermal decomposition.

2.2.4 Use of Nitrogen Purged Brewster Angle Windows on the Staged Combustion Device.

The results from Section 2.2.3 again indicate that the NF_2 is the limiting reagent in the system, and on the time scale of the supersonic flow, N_2F_4 thermal decomposition is slow.

All of the previous experiments were done with flat sapphire windows which require no purge gas flow. For such a small laser device, the N_2 purge gas associated with CaF_2 brewster windows is known to increase the cavity pressure by a significant fraction. This subsonic gas flow compressing the main HF-NF flame from the sides has the effect of increasing the temperature as well as pressure of the flow field. In this way, the purge flow acts like a shroud causing some of the supersonic gas flow energy to be released to gas enthalpy instead of free jet expansion. The overall effect should be an increase in reaction rates including N_2F_4 thermal decomposition and a shortening of the reaction zone length.

This hypothesis was tested by the addition of CaF_2 brewster windows in place of the two flat sapphire windows closing the lasing axis in the upstream

viewing cell. The results are shown in Figures 18 and 19. In Figure 18, the NF(b) signal at $X_c' = 2.0$ cm was observed as a function of N_2 purge flow. The cavity pressure rises continuously with N_2 flow. The NF(b) signal first drops, then rises to about three times its original signal level. This initial decrease may represent a fall in $HF(v \geq 2)$ concentration as a result of V-T deactivation at the increased cavity pressure. The overall increase in NF(b) intensity probably reflects increased N_2F_4 thermal decomposition. These measurements were made for Case 27 conditions including NO flow as indicated in Table 8. The N_2F_4 flow was 0.20×10^{-3} mol/sec for these runs due to diminishing N_2F_4 supply. The N_2 purge flow does not appear to substantially alter the flame. The flame is more intense close to the secondary blade and some pinching in from the sides is observed.

Figure 19 shows the variation in NF(a) and NF(b) intensity as a function of X_c'. The experimental conditions here are identical to those in Figure 17 except for the addition of brewster windows with a N_2 purge flow of 28.4×10^{-3} mol/sec, and a N_2F_4 flow of 0.20×10^{-3} mol/sec. Both the NF(a) and NF(b) have increased, and a maxima is observed for both within the viewing region. The NO flow has a signal enhancement effect on the NF(b) signal unlike the previous situation without the N_2 purge. While the increase of signals observed between Figures 17 and 19 is not large, being about a factor of two or three, this does lend evidence that the N_2F_4 is not fully dissociating. A preliminary analysis indicates that the NF(a) signal is about a factor of fifty less intense than would be expected if the N_2F_4 was fully dissociated and there were no significant deactivation channels for NF(a).

2.2.5 Quantitative Measurement of NF($a^1\Delta$) and ($b^1\Sigma^+$) Population Densities

The assumptions have been made that there is a substantial amount of H-atoms and $HF(v \geq 2)$ in the flow field, and that the gas temperature is high enough (> 600°K) to dissociate N_2F_4. The goal of the final set of staged combustion experiments is to quantitatively determine the concentration of the gas species including NF(a) and NF(b) so that the limitation which results in less than anticipated NF excited state intensities can be identified. It is preferable to work at conditions which maximize both NF(a) and NF(b) population, so the experiments will use the purged brewster windows. Nitric Oxide will be mixed with the H_2 cavity fuel to delineate

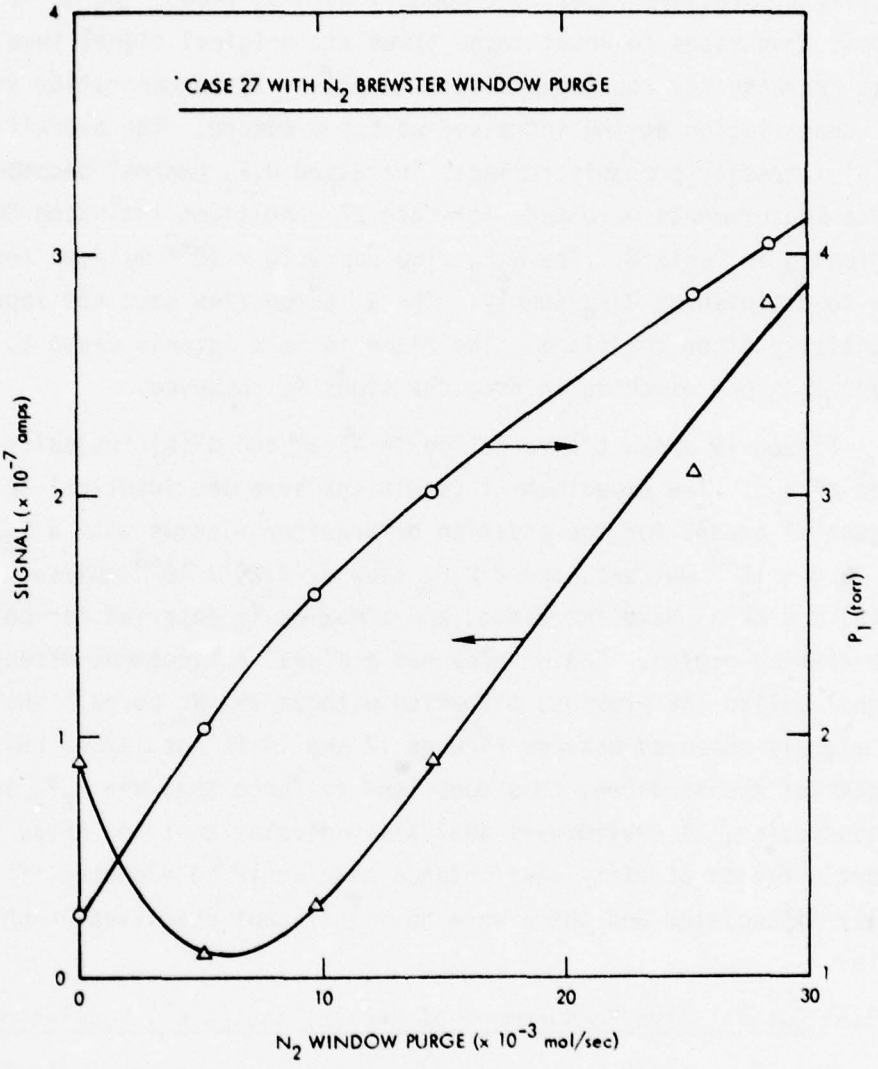

Figure 18. Cavity Pressure P_1 and $NF(b^1\Sigma^+)$ Signal at $X_c' = 2.0$ cm Versus N_2 Window Purge Flow Rate. For Case 27 as Given in Table 8 Except N_2F_4 is 0.20×10^{-3} mol/sec.

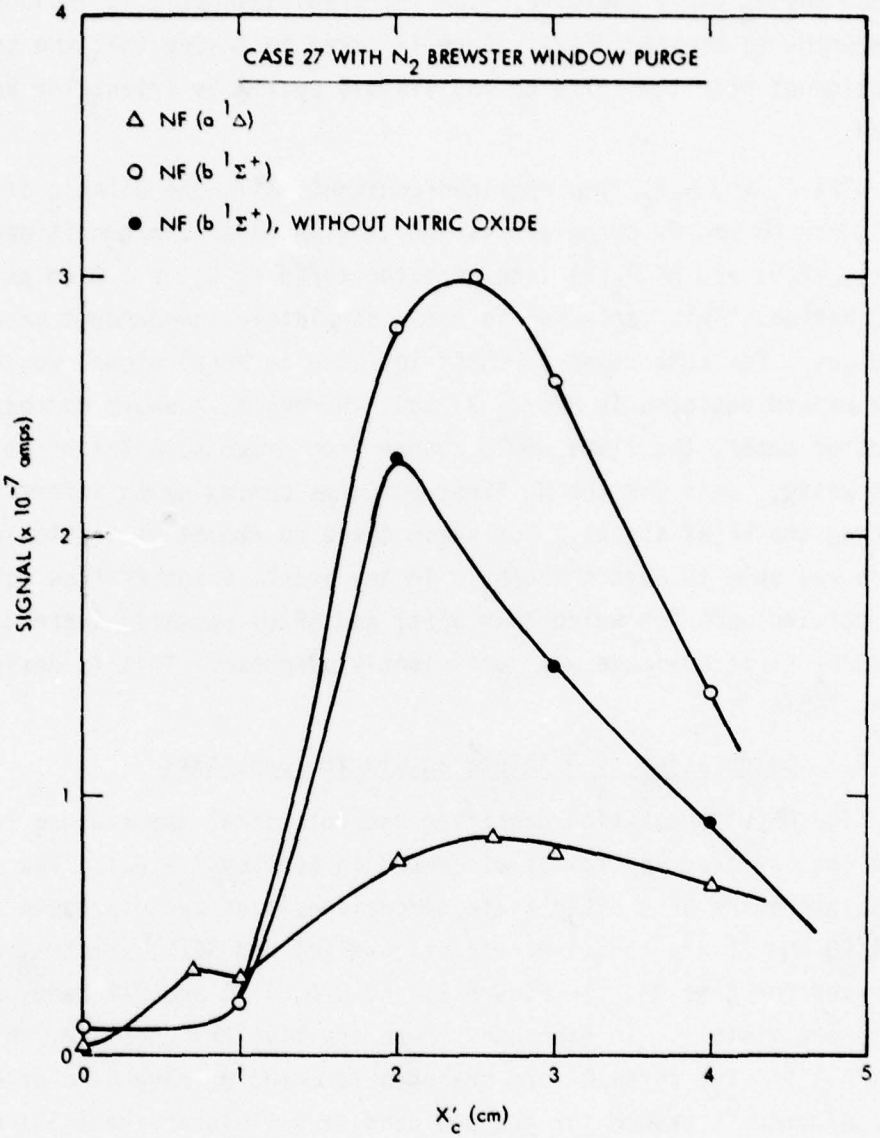

Figure 19. NF($a^1\Delta$) and ($b^1\Sigma^+$) State Intensity Versus X'_c for N_2 Window Purge Case. H_2 and NO in Primary Busemann Injector and N_2F_4 in Secondary Wedge Injector. Experimental Conditions for Case 27 Given in Table 8 Except N_2F_4 Is 0.20 x 10^{-3} mol/sec. N_2 Purge Flow Is 28.4 x 10^{-3} mol/sec. Cavity Pressure P_1 Is 4.04 torr.

the NF(a) spectra. It is assumed that the NO has little effect except to quench the N_2 first positive. The infrared diagnostic is included in this experiment to monitor HF(v). Care is taken to insure that the spectral function of both the infrared and visible system is triangular and of known width.

The F_2 and N_2F_4 flow remained constant while the balance of the gases including NO and N_2 purge are varied to give favorable conditions. The NF(a), NF(b) and HF $P_2(6)$ line were monitored at $X_c' = 2.0$ cm as the gases were varied. This variation is not a completely independent process for each gas. For some cases a modest increase in NF(a) signal would result in a marked decrease in HF($v \geq 2$) and, therefore, a sharp decrease in NF(b). In other cases, the flame would change from green to a bright yellow, almost white. This was the N_2 first positive coming up in intensity and obscuring the NF(a) signal. For these cases no amount of available nitric oxide was able to quench the N_2. In any event, a set of flow conditions was settled upon for which both NF(a) and NF(b) appeared intense, and for which N_2 first positive was sufficiently quenched. This is designated Case 38 in Table 8.

2.2.5.1 Calculation of Absolute Population Densities

The HF(v) population densities and rotational temperature result from the infrared spectra as discussed in Section 2.1.3.1. The details of calculating the NF excited state number densities are discussed here. Figures 20 and 21 are the high resolution NF(a) and NF(b) spectra, respectively, observed for Case 38. In Figure 21 the 0-0, 1-1, and 2-2 bands of NF($b^1\Sigma^+ \rightarrow X^3\Sigma^-$) are visible. In each band there are five branches; ${}^{O}P$, ${}^{Q}P$, ${}^{Q}Q$, ${}^{Q}R$, and ${}^{S}R$.[12] The three Q-form branches form the primary head of each band. The unformed ${}^{O}P$ branch for the 0-0 band is visible at about 531 nm. The 0-1 (562 nm) and 1-2 (560 nm) bands were also observed but at a much reduced intensity. The spectral resolution is such that individual vibration-rotation lines are not resolved. The NF(b) population density is obtained from the spectra in Figure 21 in the following manner.

The monochrometer entrance and exit slits are the same width (and height) and a triangular slit function is appropriate. With the monochrometer set at λ_o, the relative contribution from light between $\lambda + d\lambda$

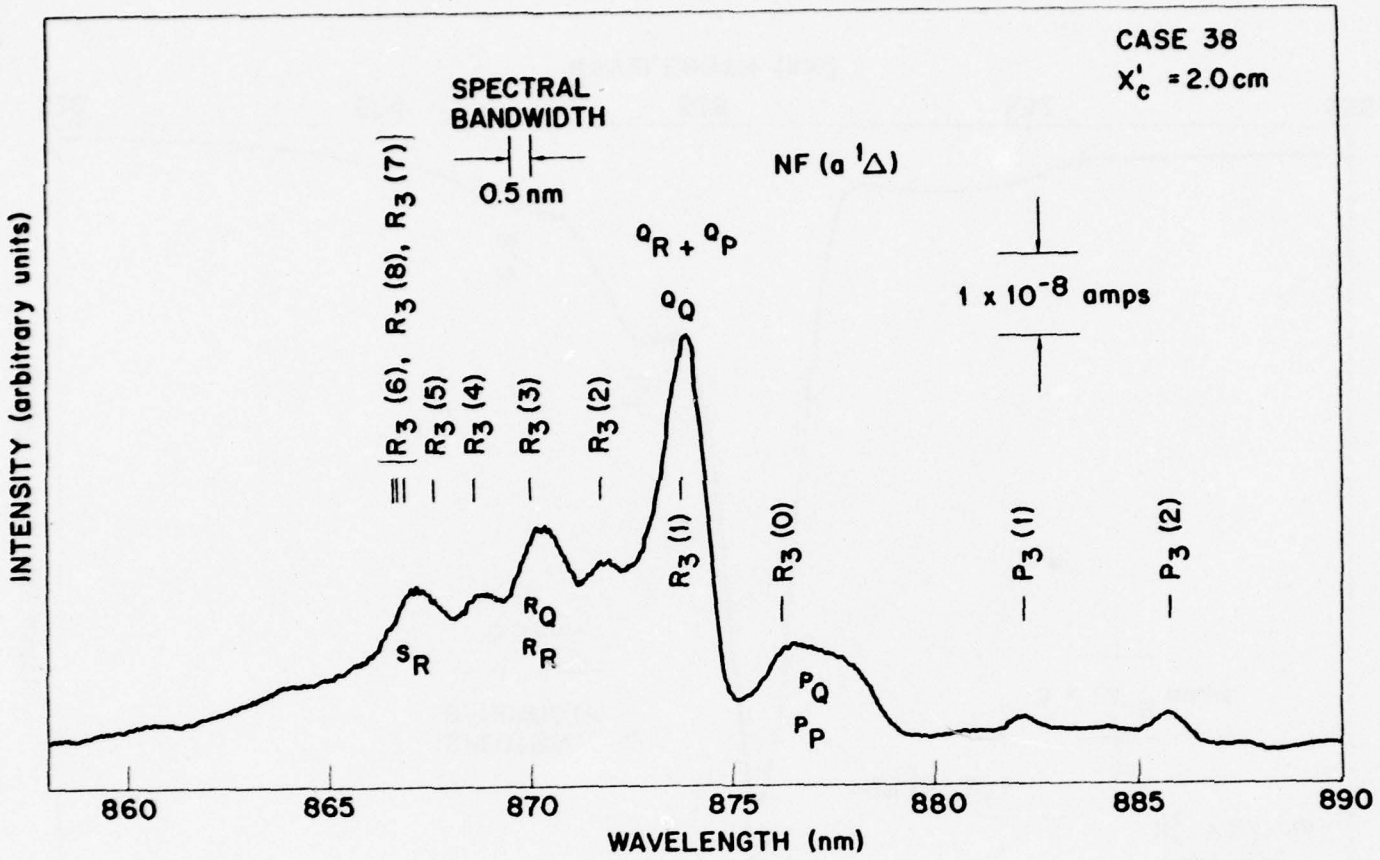

Figure 20. NF($a^1\Delta \rightarrow X^3\Sigma^-$) 0-0 Band Emission. The Various P_3 and R_3 Lines Indicated in the Spectrum Are the Wavelength Positions for HF($v = 3 \rightarrow 0$, J) Transitions.

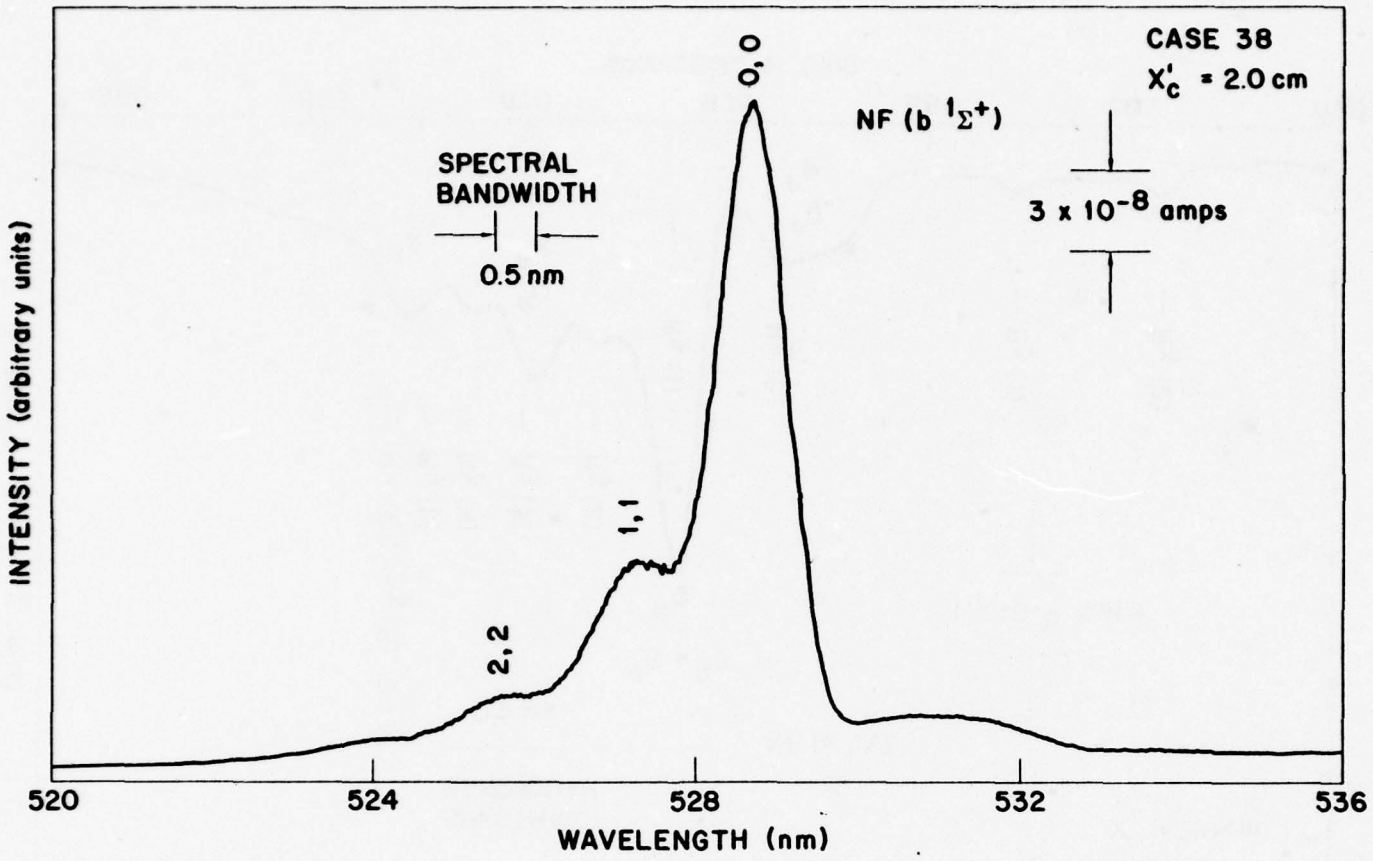

Figure 21. NF($b^1\Sigma^+ \rightarrow X^3\Sigma^-$) $\Delta v = 0$ Emission Bands.

due to this slit function is

$$S(\lambda,\lambda_0)d\lambda = [1 - |\lambda-\lambda_0|/FWHM]d\lambda \quad (15)$$

for $|\lambda-\lambda_0| \leq FWHM$, and $S(\lambda,\lambda_0) = 0$ elsewhere, where FWHM is the instrumental full width at half maximum due to the finite slit. When the standard Eppley lamp is used to calibrate the detection system, the amperes of signal observed at the output of the photomultiplier tube (PMT) with the monochrometer set at λ_0 is

$$amps(\lambda_0) = 1.6 \times 10^{-19} \int N(\lambda) \cdot A \cdot S(\lambda,\lambda_0) \cdot T(\lambda) \cdot QE(\lambda) \cdot G \cdot d\lambda \quad (16)$$

where $N(\lambda)$ is the photons/cm^3-sec-nm produced by the Eppley lamp at wavelength λ at the entrance slit of the monochrometer, A is the slit area, $T(\lambda)$ is the spectrometer and associated optics transmission at λ, $QE(\lambda)$ is the quantum efficiency of the PMT photocathode, and G is gain of the PMT. It is assumed that the wavelength dependence of $N(\lambda)$, $T(\lambda)$, and $QE(\lambda)$ is much slower than is $S(\lambda,\lambda_0)$. Equation 16 simplifies to

$$amps(\lambda_0) = 1.6 \times 10^{-19} \cdot A \cdot G \cdot N(\lambda_0) \cdot T(\lambda_0) \cdot QE(\lambda_0) \int S(\lambda,\lambda_0)d\lambda \quad (17)$$

$$= 1.6 \times 10^{-19} \cdot A \cdot G \cdot N(\lambda_0) \cdot T(\lambda_0) \cdot QE(\lambda_0) \cdot FWHM \quad (18)$$

$amps(\lambda_0)$ is taken from a calibration spectra done with the Eppley lamp, $N(\lambda_0)$ from the NBS traceable Eppley lamp calibration and the energy of photons with wavelength λ_0, and FWHM is determined experimentally using a line source much narrower than the slit function (e.g., a laser or an HF($\Delta v = 3$) vibration-rotation line). A wavelength dependent calibration constant $C(\lambda_0)$ can be written in terms of known quantities

$$1.6 \times 10^{-19} \cdot A \cdot G \cdot T(\lambda_0) \cdot QE(\lambda_0) = amps(\lambda_0)/[FWHM \cdot N(\lambda_0)] \quad (19)$$

$$= C(\lambda_0)$$

A, the slit area, is kept on the left hand side of Equation 19 for convenience, although it is known.

The identical optics/spectrometer/detector system is used to observe the NF signal. Let $I(\lambda)$ be the photons/cm^2-sec-nm produced by the NF excited state emission at the entrance slits at wavelength λ. The signal $X(\lambda_o)$ in amps observed at the wavelength λ_o is then

$$X(\lambda_o) = 1.6 \times 10^{-19} \cdot A \cdot G \cdot T(\lambda_o) \cdot QE(\lambda_o) \int I(\lambda) \cdot S(\lambda, \lambda_o) d\lambda \quad (20)$$

$$X(\lambda_o) = C(\lambda_o) \int I(\lambda) \cdot S(\lambda, \lambda_o) d\lambda \quad (21)$$

In Equation 21, $X(\lambda_o)$ is the measured spectrum which results from the actual spectrum $I(\lambda)$ convoluted by the slit function. $C(\lambda_o)$ is known from the previous calibration.

The spectral resolution for these experiments was chosen to provide a balance between measured signal levels and sufficient resolution to clearly identify the NF(a) and NF(b) spectrum as well as interfering spectral features from other molecules. Since the observed emission features have about the same order width as the slit function, Equation 21 must be integrated numerically to obtain the integral of the absolute photon flux. Since $C(\lambda_o)$ is approximately constant over the emission spectrum, integration of Equation 21 over λ_o gives

$$\int X(\lambda_o) d\lambda_o = C(\lambda_o) \int I(\lambda) \int S(\lambda, \lambda_o) d\lambda_o d\lambda \quad (22)$$

$$= C(\lambda_o) \cdot FWHM \int I(\lambda) d\lambda \quad (23)$$

$$\int I(\lambda) d\lambda = \int X(\lambda_o) d\lambda_o / [C(\lambda_o) \cdot FWHM] \quad (24)$$

That is, the integral of the observed spectrum done with a planimeter is related simply to the integral of the absolute photon flux.

For the NF(b) state emission spectra in Figure 21, the integrated absolute photon flux can be converted to emitter number density by

$$[NF(b^1\Sigma^+)] = \frac{\tau_b}{f \cdot L} \int I_b(\lambda) d\lambda \quad (25)$$

where τ_b is the radiative lifetime 0.015 sec for the NF($b^1\Sigma^+ \rightarrow X^3\Sigma^-$) band[7] and L is the optical path length. The integrated photon flux $\int I_b(\lambda)d\lambda$ for NF(b) is derived for the entire experimental $\Delta v = 0$ spectrum from v' = 0 to n, but it is still necessary to account for the $\Delta v = -1$ spectra not included in the integration. This is done by dividing by the Frank Condon factor, f = 0.9, for the $\Delta v = 0$ bands. In this way, the NF(b) state population density obtained in Equation 25 is summed over all vibrational levels which are observed to be populated for the $b^1\Sigma^+$ electronic state.

The NF($a^1\Delta$) population density is obtained in an identical manner except for two minor differences. First, only the 0-0 band of the NF($a^1\Delta \rightarrow X^3\Sigma^-$) is observed in Figure 20. The main head at 874.2 nm is made up from three Q-form branches.[14] Eight of the nine branches possible for this band are identified in Figure 20. No $\Delta v = 0$ bands from v' > 0 are observed, however they may be weakly underlying the observed spectra. Bands from $\Delta v = -1$ have not been observed by us or others.[14] The result is that for the NF($a^1\Delta$) population density, a Frank Condon factor is not used in the Equation

$$[NF(a^1\Delta)] = \frac{\tau_a}{L}\int I_a(\lambda)d\lambda \qquad (26)$$

where τ_a is an estimate[8] for the NF($a^1\Delta \rightarrow X^3\Sigma^-$) radiative lifetime of 0.7 sec, L is the optical length, and $\int I_a(\lambda)d\lambda$ is the integrated photon flux of the observed NF(a) emission spectrum obtained from Equation 24.

The second difference concerns the HF(v = 3 → 0) lines which interfere slightly with the NF(a) emission. These HF lines are shown in Figure 20, but at these flow conditions the NF(a) is more intense. Figure 22 is for the identical conditions except D_2 has been substituted for the H_2 cavity fuel. Comparing Figures 22 and 20, it is a simple matter to integrate out by "eye" the interfering HF spectra. This is further aided by the observation of the magnitude of the HF $P_{3 \rightarrow 0}(1)$ and $P_{3 \rightarrow 0}(2)$ lines. These lines fall in a region where no NF(a) emission is present and the lines give a quantitative estimate to the magnitude of the HF R-branch lines. This correction for the presence of the HF R-branch lines is made when integrating the observed NF(a) emission spectrum for use in Equation 24.

One final point concerns the N_2 first positive emission. As can be

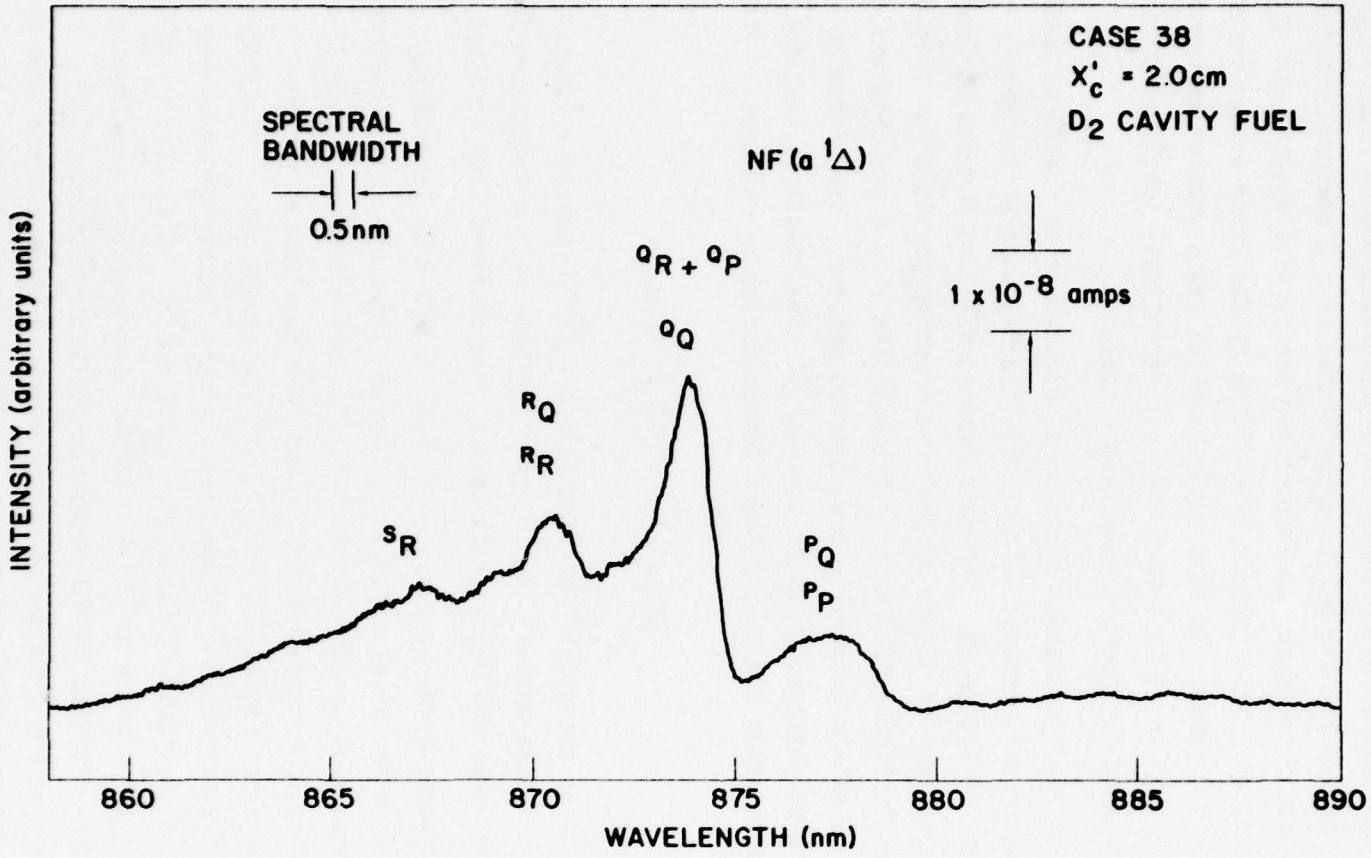

Figure 22. NF($a^1\Sigma \rightarrow X^3\Sigma^-$) 0-0 Band Emission for Case Using Deuterium Cavity Fuel.

seen in Figure 20, the region between the well resolved HF $P_{3 \rightarrow 0}(1)$ and $P_{3 \rightarrow 0}(2)$ lines has returned to the zero signal level. This would be a region where the N_2 emission would normally be seen when present in sufficient intensity to interfere with the NF(a) spectrum. In practice, for all the NF(a) spectral scans, observation was extended through this region to observe both the intensity (or lack of) for the HF P-branch lines and N_2 first positive bands.

2.2.5.2 Results

Figure 23 shows the variation in the NF(a), NF(b) and HF $P_{2 \rightarrow 1}(6)$ intensity with X_c' for Case 38. The slits are considerably more narrow (0.5 nm) than for the previous experiments, so the signal magnitudes cannot be compared directly. There is an induction period until $X_c' = 0.5$ cm before substantial reaction or mixing takes place. After that point, both the NF(a) and NF(b) rise sharply. The NF(b) has a definite maximum at $X_c' = 2.0$ cm, and falls after that point. This is probably due mostly to a decrease in HF($v \geq 2$) concentration. In contrast, the NF(a) signal levels off and only slowly decreases with X_c'. This behaviour is followed by the flame. With the NO flow on, the bright green flame is observed only in the upstream cell. In the downstream cell ($X_c' = 10.6$ to 16.8 cm) no green flame is observed indicating that the NF(b) is no longer being produced at large X_c. In fact, there must be a quenching mechanism to decrease NF(b), probably the near resonant E-V energy deactivation by HF($v = 0$).

With the NO flow off, the entire viewing region, even downstream of the second viewing cell, is a bright yellow flame. The yellow flame remains the same even when D_2 cavity fuel is used. NF(a) and H or D-atoms are necessary in the steps leading to the N_2 first positive emission (see reactions 13 and 14 above), and the short radiative lifetime ($\tau \approx 5$ μsec) of the $N_2(B^3\Pi_g)$ state means that the yellow flame is essentially a tracer for NF(a) and excess H-atoms. The extent of the yellow flame means that excess H-atoms persist far downstream, and NF(a) is either continually produced or has minimal reaction/deactivation over a long flow distance. The gradual decrease of NF(a) in Figure 23 would indicate that fast reaction/deactivation processes are not probable for NF(a).

It was not possible to make a spectral scan at all the points indicated

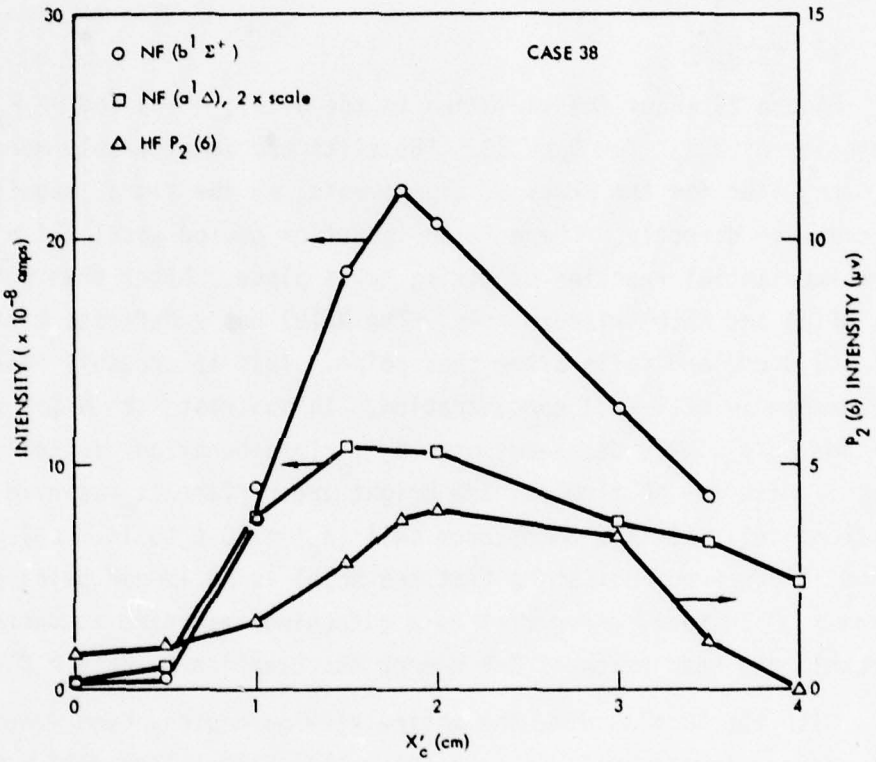

Figure 23. NF($b^1\Sigma^+$), NF($a^1\Delta$), and HF $P_{2\rightarrow1}(6)$ Peak Emission Intensity Versus X'_c for Case 38 Conditions.

in Figure 23. Figure 24 does show that the integrated intensity of the experimental spectrum does follow the trend shown by the peak intensity values in Figure 23. The values for NF(a) and NF(b) population density derived from Figure 24 at $X_c' = 2.0$ are given in Table 9.

Figure 25 shows the results of the simultaneous infrared measurements. The HF($v \geq 2$) concentration is on the order of 2×10^{14} molec/cm^3 throughout the reaction region until it drops sharply after $X_c' = 3.0$ cm. This means there should be sufficient vibrationally excited HF available for V-E energy transfer with NF(a) to form NF(b). A sharp drop in NF(b) would be anticipated beyond $X_c' = 3.0$ cm. The drop in NF(b) after $X_c' = 2.0$ cm noted in Figure 23 may indicate the already declining value of NF(a) concentration as well as HF($v = 3$). The HF($v = 3$) is more nearly resonant than HF($v = 2$) for the V-E energy transfer process. The lack of any NF(b) observed in the downstream cell certainly reflects the complete deactivation of HF($v \geq 2$) and a corresponding rise in HF($v = 0$).

While there is no measurement of the HF($v = 0$) concentration, it is estimated to be about 4×10^{15} molec/cm^3 at $X_c' = 2.0$ cm. The cavity pressures are high enough to expect a significant deactivation of HF(v) to the ground state. This would mean that the observed ratio of NF(a) to NF(b) of 30/1 is very nearly the equilibrium concentration expected at 1000°K for the given HF(v) concentrations.

The rotational temperature given in Figure 25 indicates a gas temperature of about 1000°K. This should be more than adequate to dissociate the N_2F_4 at equilibrium. Since to a first approximation $[H] = \sum_v [HF(v)] \cong 5 \times 10^{15}$ molec/cm, there should be a copious amount of H-atoms to react with any NF_2. The persistance of the yellow flame far downstream indicates excess H-atoms are surviving a considerable distance. If we assume that for Case 38 all of the free F_2 in the combustor is converted to F-atoms, and that all the H_2 (which is slightly less than the available F-atoms) is converted to H-atoms, the gas flows as they reach the secondary N_2F_4 injector would have the values given in Table 10. If the further assumptions are made that all the N_2F_4 dissociates, and all the NF_2 reacts with H-atoms to form NF excited states without any subsequent deactivation or reaction of NF, the gas flows downstream from the secondary blade would have the

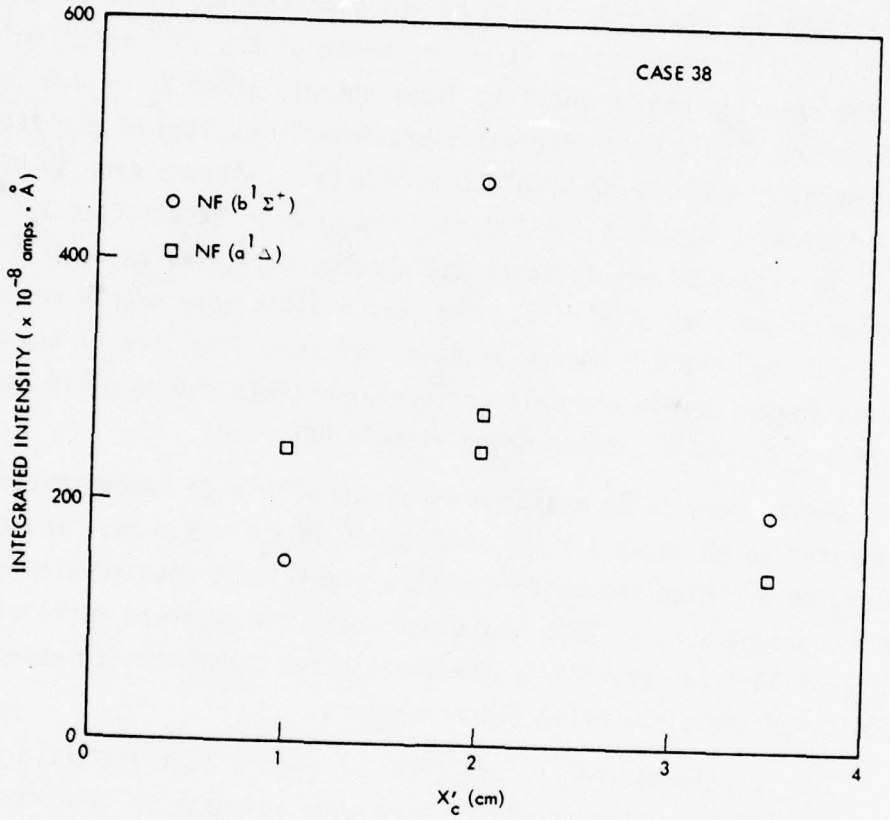

Figure 24. $NF(b^1\Sigma^+)$ and $NF(a^1\Delta)$ Integrated Emission Intensity Versus X'_c for Case 38 Conditions.

Table 9. NF Excited State Production by Staged Combustion. Results for Case 38 at X'_c = 2.0 cm.

$NF(a^1\Delta)$	6.8×10^{13} molec/cm^3
$NF(b^1\Sigma^+)$	2.3×10^{12} molec/cm^3
$HF(v \geq 2)$	1.9×10^{14} molec/cm^3
$NF(a^1\Delta)/NF(b^1\Sigma^+)$	30/1, Equilibrium Ratio
N_2F_4 Dissociation Efficiency	1%
Gas Pressure	6.1 torr
Gas Temperature	985°K
Linear Flow Velocity	4×10^4 cm/sec

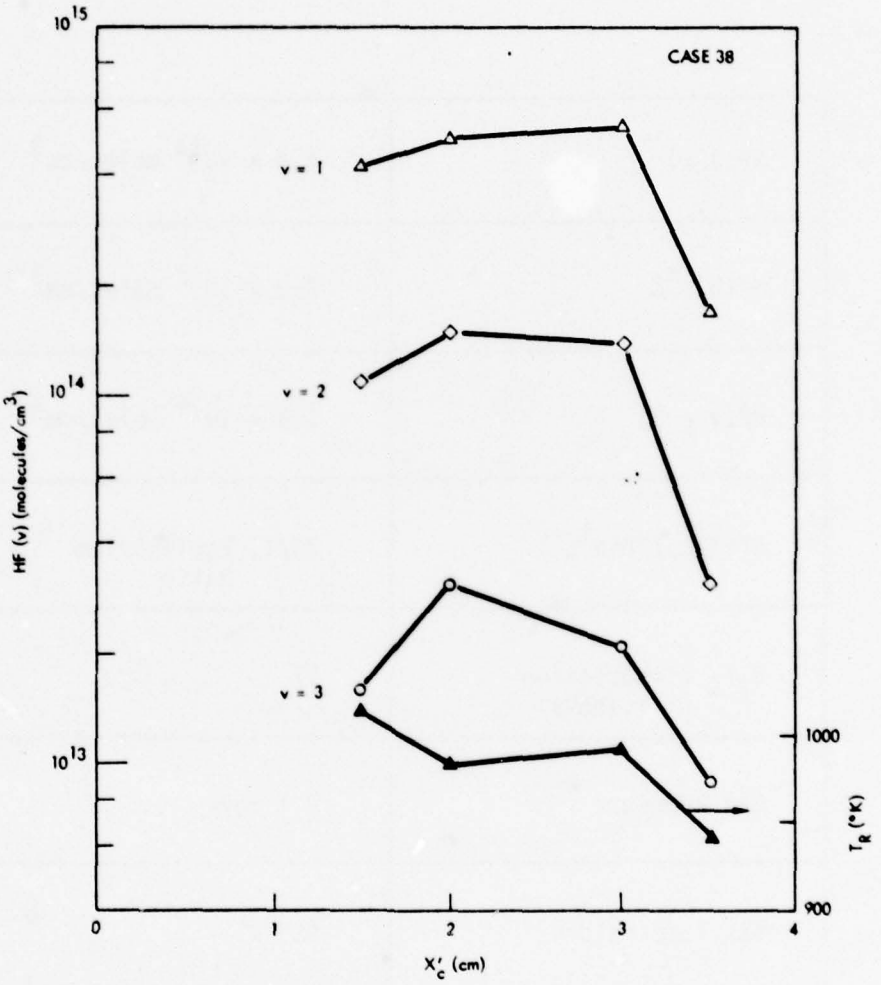

Figure 25. HF(v) Population Density and Rotational Temperature Versus X'_c for Case 38 Conditions.

Table 10. Case 38 Gas Flows Upstream of Secondary Injector.

Gas	Flow (x 10^{-3} mol/sec)
He	5.5
DF	3.5
F	0.2
H	1.8
$\sum_{v}$HF(v)	1.8
NO	2.2

Table 11. Postulated Best Case NF Gas Flows Downstream of Secondary Injector for Case 38.

Gas	Flow (x 10^{-3} mol/sec)
He	5.5
DF	3.5
F	0.2
H	0.8
$\sum_{v}$HF(v)	2.8
NF*	1.0
NO	2.2

values in Table 11. The N_2 purge gas flow is not included in Table 11 since it does not mix with the flame gases, but rather only provides a confining sheath flow. From the measured pressure and temperature in the cavity, the mole fraction of total NF* excited states in this most optimistic case would correspond to a concentration of about 3.8×10^{15} molec/cm^3. The sum of NF excited states measured for Case 38 at X_c' = 2.0 cm corresponds to 2% of this maximum amount. This would correspond only to one percent dissociation of N_2F_4 if all the subsequent NF_2 was utilized with complete efficiency.

This NF_2 utilization rate of two percent is a lower bound and given the level of the various assumptions of perfect mixing and reaction, the N_2F_4 dissociation is probably more in the one to three percent range. This is still considerably lower than what is expected at 1000°K. However, a low NF_2 concentration explains the low concentration of NF(a) that is observed. The low steady state concentration of NF(a) means that the production and removal rates of NF(a) are nearly balanced. The slow decay of NF(a) concentration reflected in Figure 23 would indicate that the production rate is also low. The rate constant for the reaction of H-atoms wiht NF_2 is large at about 0.1 gas kinetic; the concentrations of H-atoms is high; the remaining cause of a low production rate is a low NF_2 concentration.

The flame cross section is estimated to be 2 cm x 3.5 cm = 7 cm^2, and this value is used to estimate the linear flow velocity in Table 9. This corresponds to a 25 μsec/cm time scale in the flow direction.

2.3 CONCLUSIONS

The main conclusions for the staged combustion experiments come from the quantitative measurements done for Case 38, and they are summarized below.

- The low concentrations of NF(a) results from low NF_2 concentrations. The bottleneck in the NF_2 production rate results from slow thermal decomposition of N_2F_4 on the supersonic flow timescale.
- NF($a^1\Delta$) and NF($b^1\Sigma^+$) can be produced in an exclusively chemical reaction, laser type device. All experimental observations are consistent with established chemical reaction mechanisms. No undue handling or materials problems were encountered.

- In a realistic chemical laser environment, the quenching of $NF(a^1\Delta)$ and $NF(b^1\Sigma^+)$ appears to be slow. The possibility exists that NF self quenching could be a factor at higher NF concentration.

- Besides the one to three percent thermal decomposition efficiency of N_2F_4 , no kinetic bottlenecks or competing reactions were encountered. Mixing of N_2F_4 appears to be homogeneous from observations of the flame.

- It is possible to produce sufficient $HF(v \geq 2)$ to efficiently transfer $NF(a^1\Delta)$ to $NF(b^1\Sigma^+)$, and to effect an equilibrium ratio between the $NF(a^1\Delta)$ and $NF(b^1\Sigma^+)$ concentrations.

The last point deserves some additional comments. The method which would probably be used to increase the N_2F_4 decomposition rate and ultimately raise the NF excited state concentrations to a value necessary for cw lasing probably entail increasing the cavity pressure. Any such pressure increase is going to rapidly deactivate $HF(v \geq 2)$. Such deactivation not only decreases the rate of the NF(a) to NF(b) transfer, but provides more HF(v = 0) to oppose this energy transfer. The best that could be hoped for would be to establish equilibrium for the process

$$HF(v = 2) + NF(a^1\Delta) \rightleftarrows HF(v = 0) + NF(b^1\Sigma^+) \qquad (27)$$

Decreased $HF(v \geq 2)$ and increased HF(v = 0) would unfavorably shift the equilibrium to $NF(a^1\Delta)$. Also the production step for NF(a) itself produces HF(v = 0).

The advantage of transferring energy from the NF(a) to NF(b) state is the factor of ten less NF(b) state concentration compared to NF(a) that is required for threshold lasing. It is unlikely, however, that for $HF(v \geq 2)$ used as the energy transfer medium, sufficient NF(b) would be generated for lasing if NF(a) is not already of sufficient concentration to lase itself.

Overall, staged combustion still appears to be a viable concept for an NF laser. The main problem to solve is the N_2F_4 dissociation, and this is a problem which may not be unique to the staged combustion laser. Some preheating of the N_2F_4 in a subsonic flow section to produce NF_2, not unlike F-atom production in a conventional combustor is envisioned. Injection of NF_2 itself into the laser should remove any kinetic bottlenecks. The staged combustion device is flexible enough that it can easily be scaled in

size by using an array of the wedge shaped injector blades rather than the single one used here.

3. TRI-STREAM NOZZLE EXPERIMENTS

The tri-stream nozzle (TSN) allows for mixing of three component gases at the throat of a slit nozzle, prior to substantial expansion. The TSN hardware has previously been used as a DF laser device,[9] and it represents a second technique for mixing the three reagents N_2F_4, H_2, and F-atoms required for the NF system. The TSN experiments were primarily designed to gather quantitative data for a given set of flow conditions to compare to previous LAMP modeling calculations performed at AFWL for the TSN.

3.1 EXPERIMENTAL

The TSN experiments are identical in almost all respects to the staged combustion experiments except for the size and configuration of the nozzle. The details of the gas handling, optical diagnostics, and data reductions techniques will be mentioned only where they differ from those described in Section 2.0. The main concern in the TSN experiments is the scale of the nozzle means about a factor of fifty higher N_2F_4 flow, and, therefore, rapid scan techniques must be utilized to record data in a short time period. These details will be discussed below.

3.1.1 Experimental Apparatus

The experimental apparatus is shown scheimatically in Figure 26. Figures 27 to 29 show several views of the experiment. The mixing block B4 of the smallest element size (L_e = 0.24 cm) and the C3 contour nozzle with area expansion ratio A/A* = 10 are used for all experiments.

The order that the various gases issue from the mixing channels in the nozzle throat has the pattern

$$F, N_2F_4, H_2, N_2F_4, F, N_2F_4, H_2, N_2F_4, F.$$

F represents the combustor flow which contains fluorine atoms along with He and DF. The N_2F_4 and H_2 are injected as pure gases without dilution. The element length L_e is defined as the distance between the centerline of the F-atom port and the centerline of the next adjacent H_2 port. The nozzle exit dimensions are 6.35 cm x 1.02 cm, and the mixing block contains thirteen

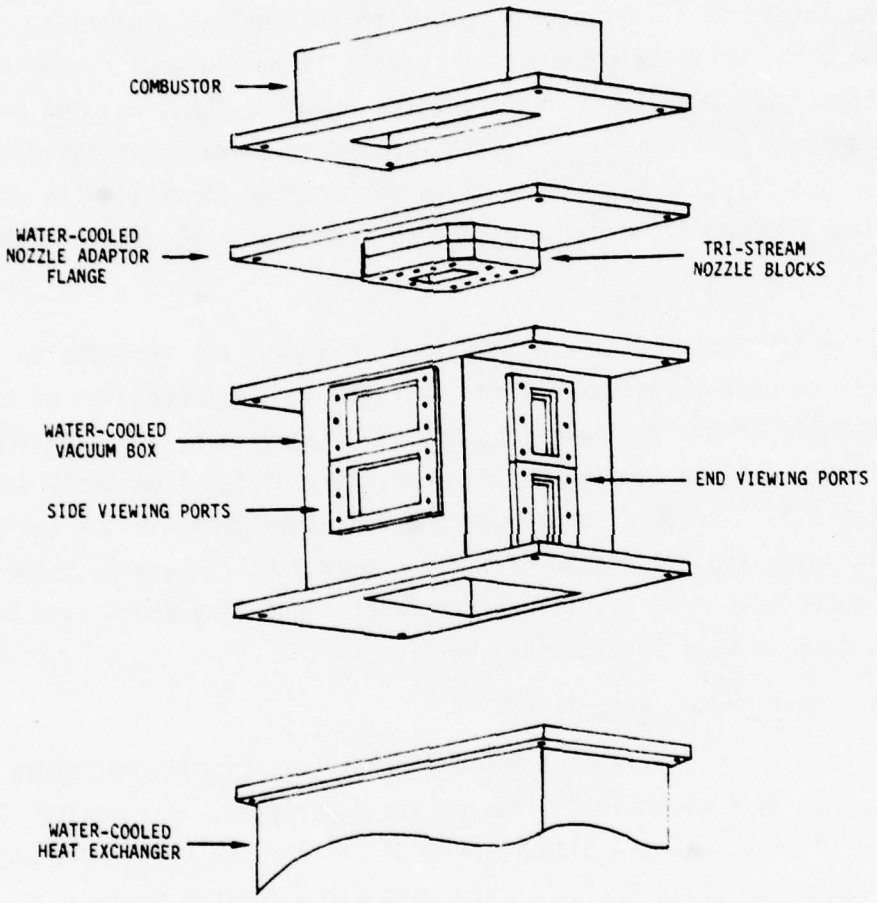

Figure 26. Tri-Stream Nozzle Experimental Apparatus.

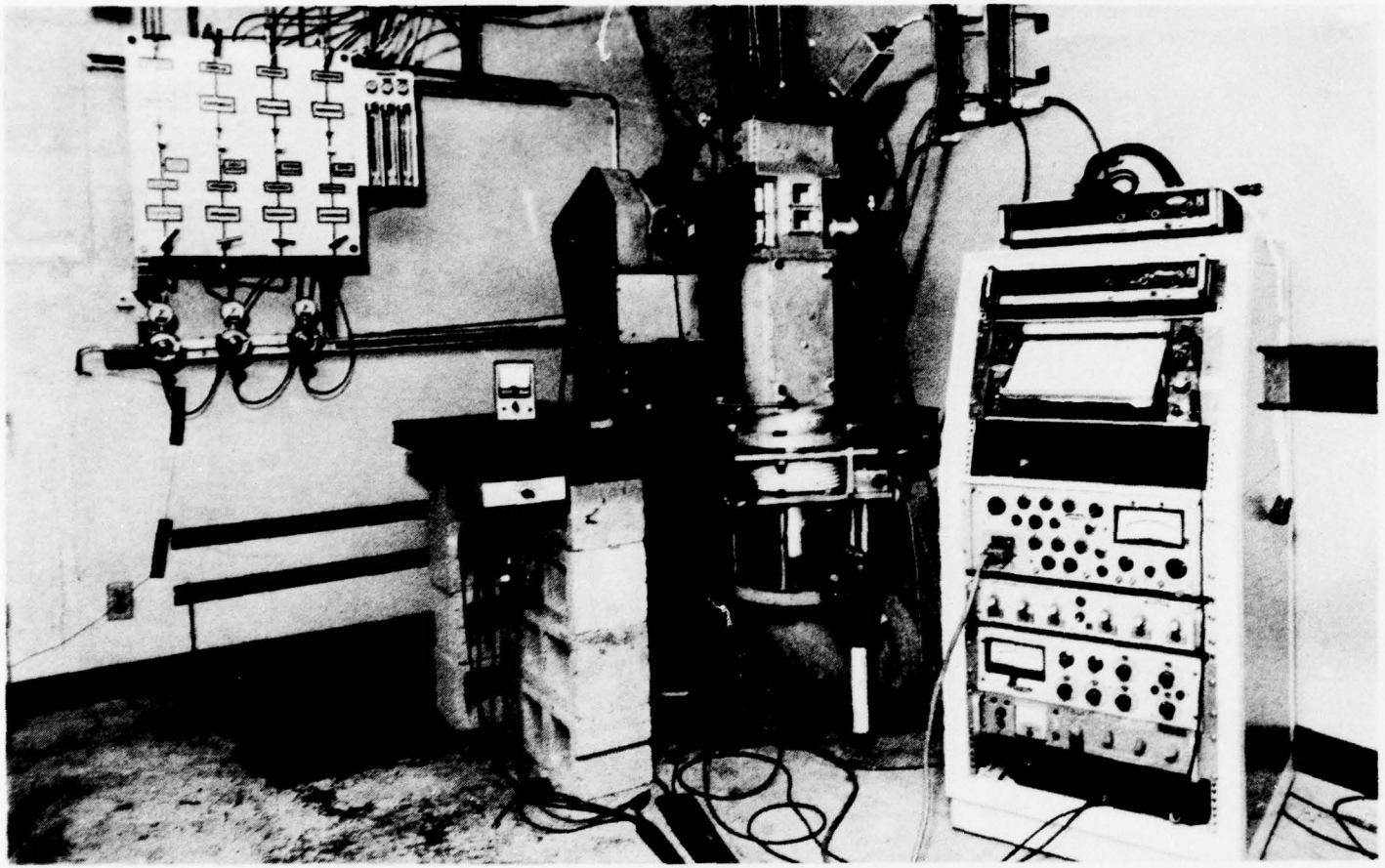

Figure 27. Overall View of Tri-Stream Nozzle Experiment. The Laser Device Is in the Center with Gas Flow from Top to Bottom. The Infrared Spectrometer Is to the Right and the Visible Spectrometer to the Left of the Laser Cavity. The Flow Control Panel Is at the far Left of the Photograph.

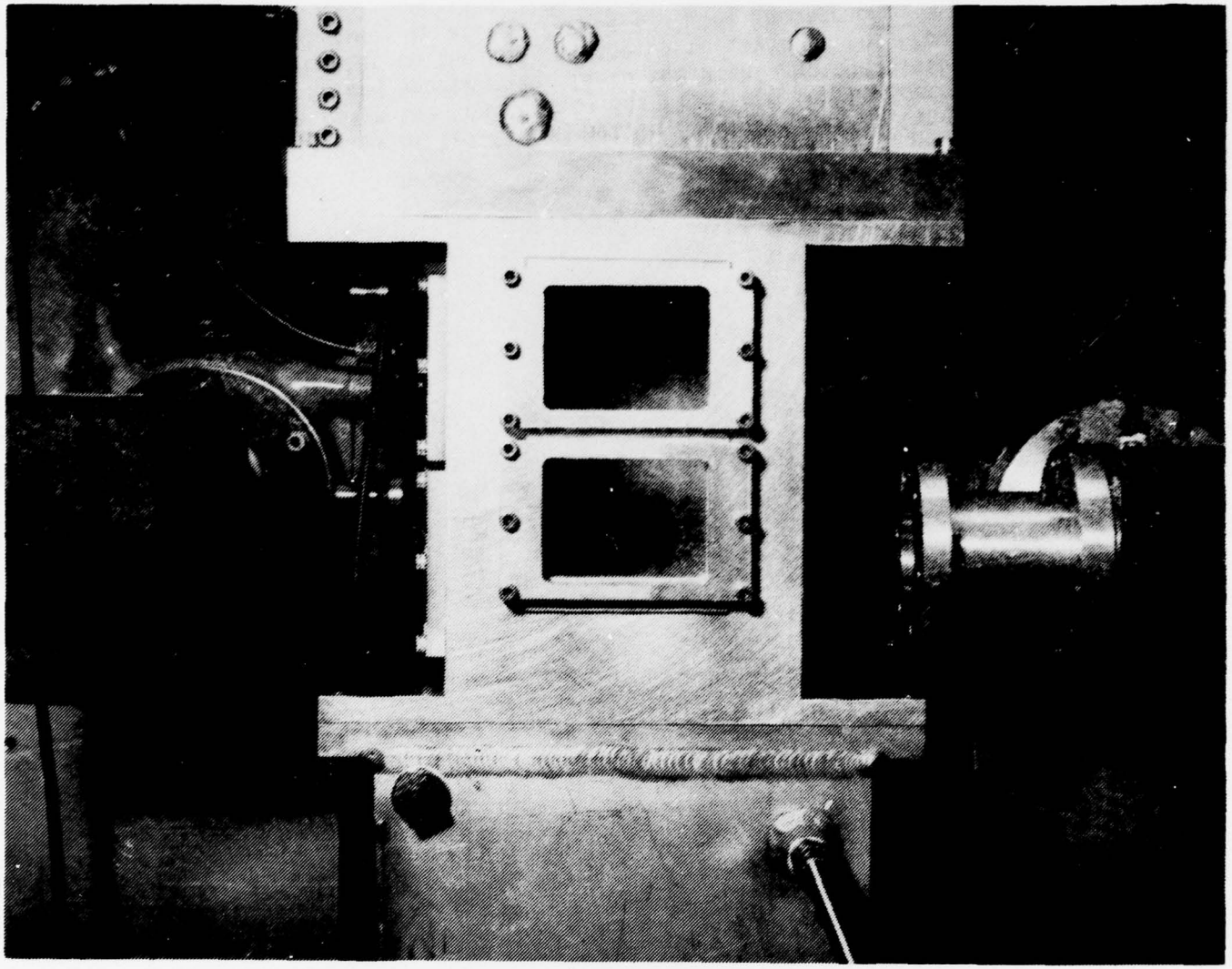

Figure 28. View Perpendicular to Laser Axis of Tri-Stream Nozzle. The Boxes Holding the Toroidal Focusing Mirror for Each Spectrometer Are at Opposite Sides of the Laser Cavity. Gas Flow is from Top to Bottom.

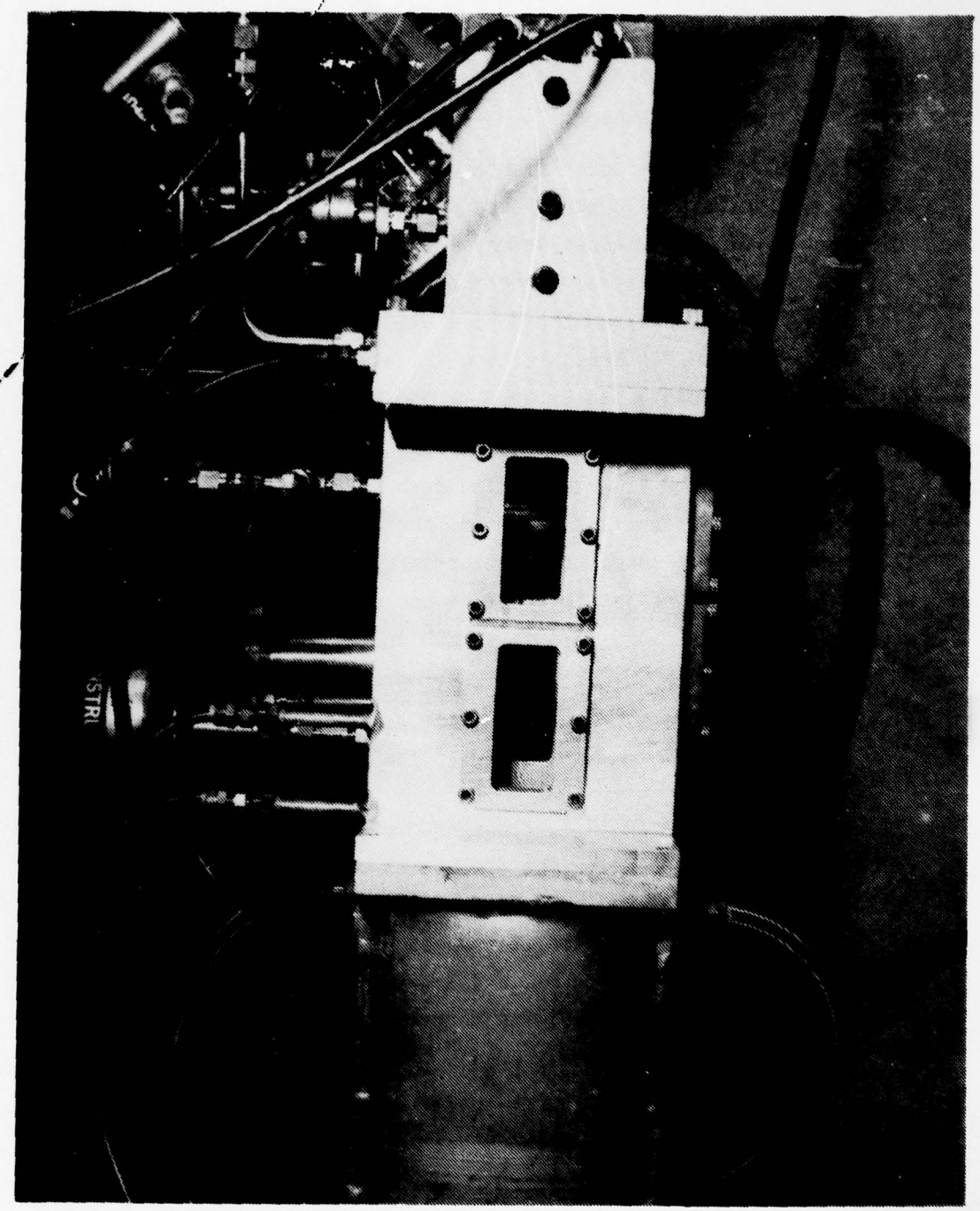

Figure 29. View Along Laser Axis of Tri-Stream Nozzle. This Is the Side that Visible Wavelength Measurements Were Made; the opposite Side Was Used for Infrared Measurements. Gas Flow Is from Top to Bottom.

F-atom ports, twenty-six N_2F_4 ports, and fourteen H_2 ports. The entire nozzle assembly is water cooled. Additional details of construction of the TSN hardware is given elsewhere.[9]

The TSN and its adaptor flange are mounted to a water-cooled vacuum box. The gases are allowed to expand free jet into the cavity. The vacuum box contains viewing windows which allow observation of the NF flame for a distance of 13 cm downstream from the nozzle exit plane. Distance along the flow axis is measured from the nozzle exit plane and designated X_c. The cavity is fitted with two pressure taps, P_1 at X_c = 0.6 cm and P_2 at X_c = 11.8 cm. 0-10 torr MKS absolute capacitance manometers are used to record the cavity pressures.

The existing MK-VI water-cooled combustor is fitted to the TSN hardware. The aluminum combustor is 15.2 cm in length and has a flow cross section of 17.8 x 3.8 cm. The combustor reactants F_2, D_2, and He are mixed by a copper shower-head impinging-jet injector at one end. The combustor pressure P_c is monitored by a Viatran 0-15 psia strain guage type pressure transducer.

The gases flow through a straight duct, water-cooled heat exhanger prior to being pumped away by the vacuum system.

3.1.2 Gas Delivery System

The F_2, D_2, H_2, and N_2F_4 flows are metered by critical flow orifices contained in a flow panel. The flow panel can be seen in Figure 27. He combustor diluent is metered by a rotometer system. All the gas flow systems have been calibrated with the test gases using Matheson linear mass flow transducers. Argon was used for F_2, and SF_6 for N_2F_4 in their orific calibrations, and the appropriate sonic orifice correction factors applied.

Of special note is the problems encountered due to large pressure drops associated with the N_2F_4 flow through the small ports in the mixing nozzle. The nozzle was originally designed for He diluent to flow through these ports,[9] and the higher molecular weight N_2F_4 encounters a substantial pressure drop. Also, the N_2F_4 is flowing into the throat of the nozzle where pressures are on the order of 0.5 atm when the other gases are on. The result is that for typical N_2F_4 flow rates, the pressure upstream of the mixing nozzle is about 0.8 atm. The result is the lower bound of the N_2F_4 pressure which is sufficient to drive the N_2F_4 flow metering orifice in a choked flow mode is 1.6 atm.

This in turn limits the amount of useable N_2F_4 in the supply bottle (N_2F_4 pressure is 7.8 atm in a full bottle). A vacuum gauge is used downstream of the orifice, and upstream of the N_2F_4 mixer to ensure that choked flow conditions are maintained.

3.1.3 Optical Diagnostics

The infrared and visible diagnostics are used in the same manner to determine HF(v), NF($a^1\Delta$), and NF($b^1\Sigma^+$) population densities and the gas temperature. All measurements are made through flat sapphire windows along the lasing axis of the nozzle (see Figure 29). A bellows and lab jack system is used to translate the spectrometers along the flow axis, and care is taken to insure that both spectrometers simultaneously view the center of the flame at the same X_c value.

The scanning speed of the visible spectrometer is set at 10 nm/sec, and the infrared spectrometer at 80 nm/sec. These scanning speeds require 5 sec to complete the NF(a) and HF(v) spectra and 2 sec to complete the NF(b) spectrum. A fast light pen Visicorder is used to record the spectra on this time scale.

It is necessary to demonstrate that at these rapid scan speeds, the time constants associated with the detector electronics and recording equipment does not distort the spectral line shape or clip some of the observable intensity. This is conviently checked prior to the NF experiments by viewing the HF flame in the TSN apparatus. The HF flame provides a number of sharp spectral lines for $\Delta v = 1$ in the infrared and $\Delta v = 3$ in the visible. At the proper time constant settings for the detector electronics, the intensity and FWHM of individual spectral lines agree with the same values at much slower scan rates. Figure 30 shows a typical HF($v = 3 \rightarrow 0$) spectrum taken at the fast scan rate.

The visible spectrometer slit height remains at 2 mm, but the infrared spectrometer slit height was increased to 4 mm because of observed signal levels. Both slits are positioned perpendicular to the flow axis. A new sensitivity calibration is determined for both the infrared and visible system immediately following the TSN experiments.

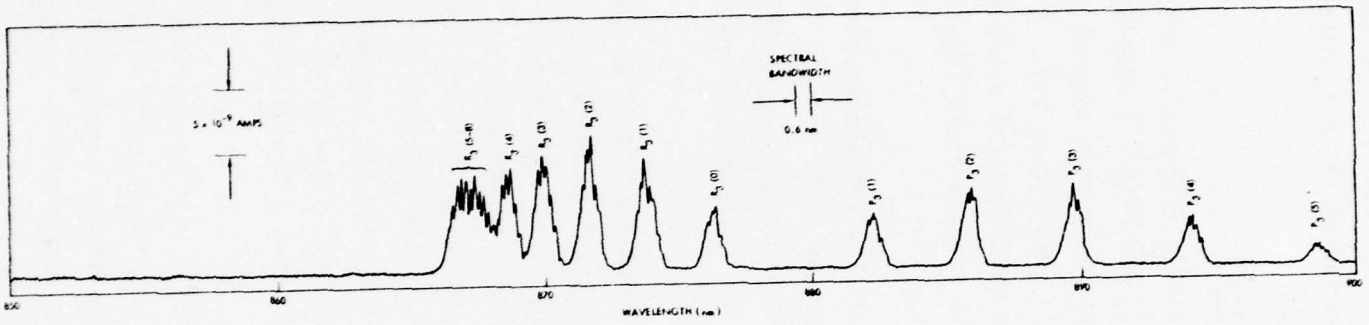

Figure 30. HF(v = 3 → 0) P and R-Branch Emission Lines from an HF Flame. Scan Time Is Five Seconds.

3.2 RESULTS

Initially, a set of flow conditions were decided upon for the experiments, and they are labeled preliminary in Table 12. These flow rates were chosen by considering the supply of N_2F_4 available, safety of handling flows in the laboratory, and flow rates and combustor pressures used in the LAMP modeling calculations.

During the course of an experimental run, the pressure upstream of the sonic metering orifice for N_2F_4 and F_2 (and, therefore, the gas flow) was monitored along with the combustor pressure P_c and the two cavity pressures P_1 and P_2. The data were recorded on fast strip chart recorders. In practice for a given run, the F_2, D_2, He, and H_2 were turned on and all checked to confirm that their nominal flow rates were correct. These flows remained constant from run to run. The N_2F_4 flow did vary slightly from run to run as the supply bottle was depleted. The recording system allowed for the actual flow during a run to be measured. The N_2F_4 would usually take 1 to 2 sec to level off after being turned on, and this was allowed to happen prior to beginning of the spectral scan. The resulting operating pressures are given in Table 12.

When preliminary gas conditions were turned on, the bright yellow flame appears throughout the cavity. Photographs from the side indicate twelve bright filaments in the flame which correspond in position to the twelve N_2F_4-H_2-N_2F_4 mixing triplets. The filaments do not seem to expand appreciably until about X_c = 5 cm, where the flame merges into a more homogeneous appearance.

Overall, the bright yellow flame seems steady, but there is an observable flickering associated with it. When either HF or NF emission is monitored this flickering is easily observable. The magnitude of this flow instability seriously degrades the signal so as to make quantitative measurement nearly impossible. Both the infrared HF and visible NF signals, coming from two separate detectors both oscillate in phase and at the same frequency (28 hz). The oscillation is present throughout the flame region, and there must be a resonant flow instability for these flow conditions. While it was possible to detect NF(a) and NF(b) emission the signal to noise ratio of about 2 to 1 precludes quantitative measurement.

Table 12. Tri-Stream Nozzle Experimental Conditions.

Case	Combustor Flows ($\times 10^{-3}$ mol/sec)			Cavity Flows ($\times 10^{-3}$ mol/sec)		Cavity Pressure (torr)		Combustor Pressure (torr)
	F_2	D_2	He	H_2	N_2F_4	P_1	P_2	P_c
Preliminary	20	10	60	20	28	1.24	1.73	654
Test	20	10	15	20	27	1.08	1.49	517

The F_2 and N_2F_4 flow were varied over a considerable range without minimizing the flow instability. Then the He flow was reduced with a marked increase in the NF signal and a disappearance of the flickering. These flow conditions now constitute the final test case conditions given in Table 12, and for which quantitative measurements were possible.

For the test case conditions, the twelve filaments are still clearly discernable from the side of the flame, but they now seem to merge at about X_c = 2.5 cm to form a homogeneous yellow flame for the balance of the viewing region. Viewed along the lasing axis, the flame appears to be a simple free jet expansion with a brighter core extending from the nozzle throat to about X_c = 2 cm.

A number of individual experimental runs were required to gather the necessary data. While the nominal conditions for the test case are given in Table 12, Table 13 gives the conditions for individual experiments. The N_2F_4 supply bottle pressure is decreasing during the course of these experiments and this is the source of the variation in N_2F_4 flow rate.

The HF(v) infrared spectrum and NF(a) visible spectrum are recorded simultaneously. Figure 31 is an example of this. This spectrum is recorded in five seconds. The NF(a) is clearly identified and the HF($v = 3 \rightarrow 0$) lines falling in the same region are labeled. In the range X_c = 1 to 5 cm, no interfering N_2 first positive emission is observed in spite of the fact that nitric oxide was not used in these experiments. The solid line passing through the NF(a) spectrum in Figure 31 encloses the area used for intensity integration of the NF(a) after correction for HF($v = 3 \rightarrow 0$) lines. The appearance of the HF($v = 3 \rightarrow 0$) spectrum is shown in Figure 30.

At $X_c \geq 8$ cm, the NF(a) and HF($v = 3 \rightarrow 0$) intensities have decreased, and the N_2 first positive emission now dominates the 870 nm region as shown in Figure 32. It was not possible to make a quantitative NF(a) measurement in this region.

Figure 33 shows the NF(b) spectrum. This scan requires 1.5 sec. The NF(b) is clearly observed throughout the viewing region.

The results for the integrated signal intensity of NF(a) and NF(b) are shown in Figure 34. Measurements between X_c = 0 to 5 cm are taken in the

Table 13. Tri-Stream Nozzle Test Case Experimental Conditions.

Experiment No.	Gas Flows ($\times 10^{-3}$ mol/sec)					Pressure (torr)			Comments
	Combustor			Cavity		Cavity		Combustor	
	F_2	He	D_2	H_2	N_2F_4	P_1	P_2	P_c	
19	20	15	10	20	27.5 — Steady	1.08	1.50	524	NF(b) Spectrum, X_c = 1 cm
20	20	15	10	20	27 — Steady	1.08	1.50	519	NF(a), HF(v) Spectrum, X_c = 1 cm
21	20	15	10	20	28.5→27.5	1.10	1.55	529	NF(a), HF(v), X_c = 3 cm
22	20	15	10	20	29.5→29	1.11	1.58	540	NF(a), HF(v), X_c = 5 cm
23	20	15	10	20	29 — Steady	1.09	1.55	527	NF(b), X_c = 5 cm, wrong Scan Speed
24	20	15	10	20	28.5→27.5	1.08	1.48	517	NF(b), X_c = 5 cm
25	20	15	10	20	27.5→27	1.06	1.45	519	NF(a), HF(v), X_c = 12 cm, Off Scale
26	20	15	10	20	27→26.5	1.08	1.50	519	NF(a), HF(v), X_c = 12 cm, N_2(B→A) Interferes
27	20	15	10	20	26.5→26	1.08	1.45	512	NF(a), HF(v), X_c = 10 cm, N_2(B→A) Interferes
28	20	15	10	20	26.5→25.5	1.08	1.45	504	Scan Did Not Start

Table 13. Tri-Stream Nozzle Test Case Experimental Conditions.
(Continued)

Experiment No.	Gas Flows (x 10^{-3} mol/sec)					Pressure (torr)			Comments
	Combustor			Cavity		Cavity		Combustor	
	F_2	He	D_2	H_2	N_2F_4	P_1	P_2	P_c	
29	20	15	10	20	26.5→25.5	1.08	1.45	506	Scan Did Not Start
30	20	15	10	20	25.5→25	1.08	1.45	512	NF(a), HF(v), X_c = 8 cm Off Scale
31	20	15	10	20	25→24	1.08	1.40	499	NF(a), HF(v), X_c = 8 cm N_2(B→A) Interferes
32	20	15	10	20	23.5→24	1.06	1.35	481	NF(b), X_c = 8 cm
33	20	15	10	20	23.5→22.5	1.05	1.43	486	NF(b), X_c = 12 cm
34	20	15	10	20	20.5→20	1.06	1.40	481	Flame Photography
35	20	15	10	20	20→19	1.05	1.33	459	Flame Photography

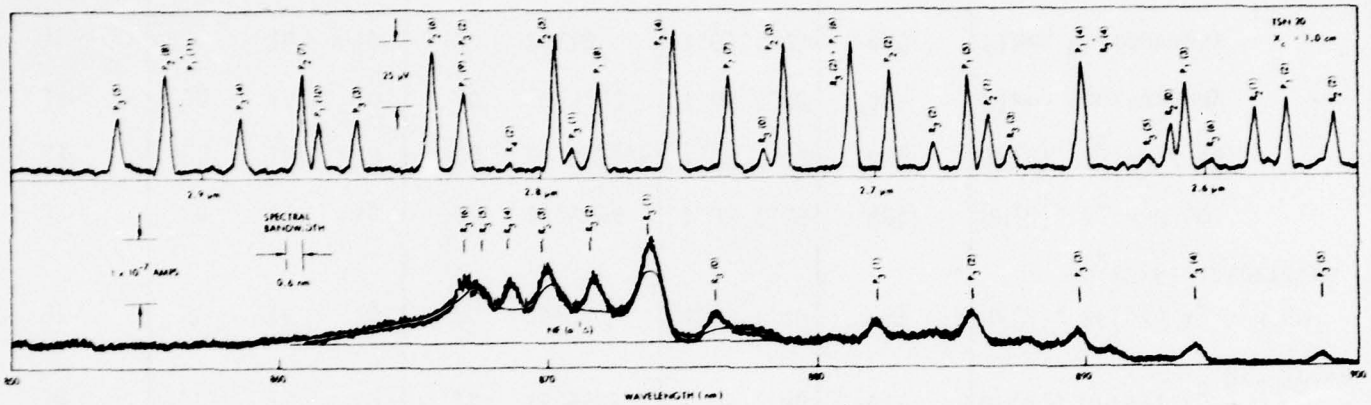

Figure 31. HF($\Delta v = 1$) Emission Lines (Upper Trace) and NF($a^1\Delta \rightarrow X^3\Sigma^+$) 0-0 Emission Band (Lower Trace) for Tri-Stream Nozzle Test Case, Experiment No. 20, $X_C = 1.0$ cm. The various P_3 and R_3 Lines Indicated in the NF($a^1\Delta$) Spectrum Are the Wave-Length Positions for HF($v = 3 \rightarrow 0$, J) Transitions. The Solid Line Drawn Through the NF($a^1\Delta$) Emission Indicates the Area Used for Measuring the Integrated Emission Intensity. Scan Time Five Seconds.

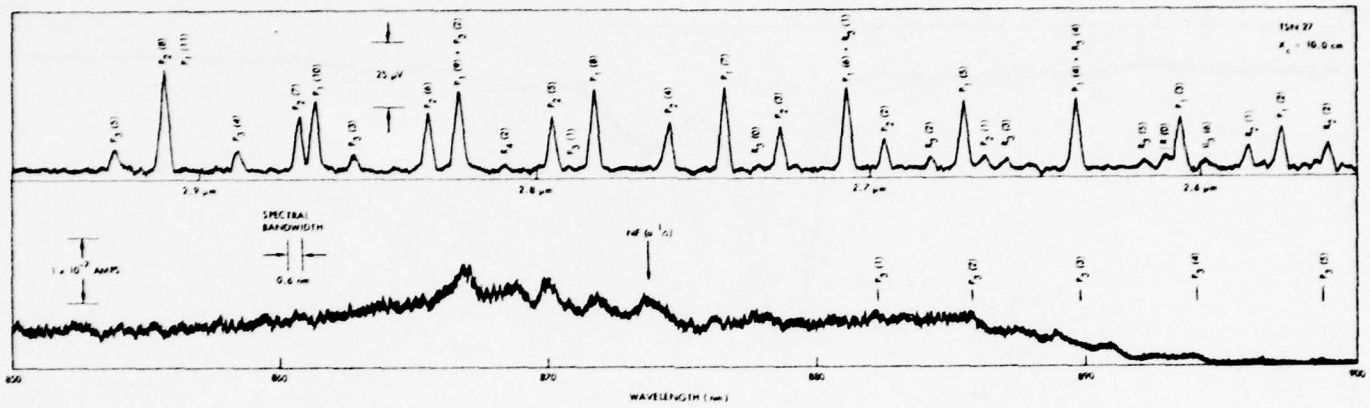

Figure 32. Same Spectrum for Tri-Stream Nozzle Test Case as Described in Figure 31 Except Experiment No. 27 X_c = 10.0 cm. The $NF(a^1\Delta)$ and HF $P_{3\rightarrow0}(J)$ Lines Are Obscured by N_2 First Positive Emission.

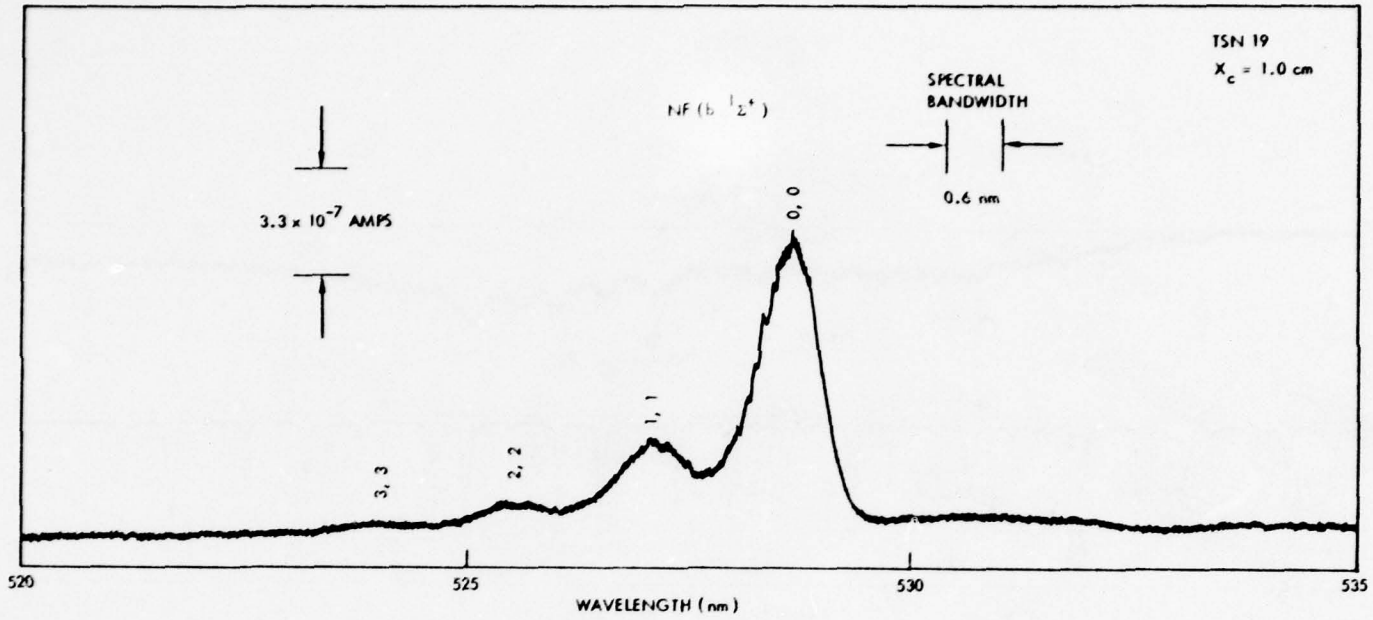

Figure 33. $NF(b^1\Sigma^+ \rightarrow X^3\Sigma^-)$ $\Delta v = 0$ Emission Bands for Tri-Stream Nozzle Test Case, Experiment No. 19, X_c = 1.0 cm. The Scan Time is 1.5 Sec.

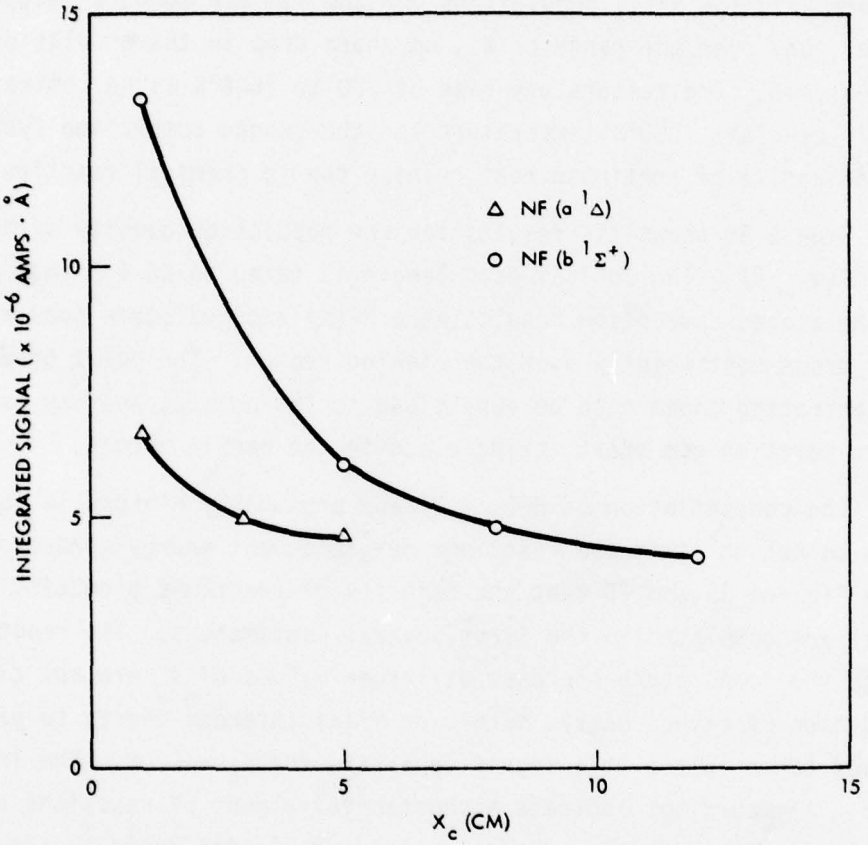

Figure 34. $NF(b^1\Sigma^+)$ and $NF(a^1\Delta)$ Integrated Emission Intensity Versus X_c for Tri-Stream Nozzle Test Case.

upstream window, between X_c = 7 to 13 cm in the downstream window. Figure 35 shows the HF(v) population density and temperature resulting from the infrared spectra. Comparing these results to the staged combustion device (Figure 25), the HF(v) populations for the TSN are about a factor of five higher, and over the range of X_c, no sharp drop in the population density is measured. The temperature rise of 700 to 1600°K is in contrast to the nearly constant 1000°K temperature for the staged combustion system, and is indicative of continued heat release due to chemical reaction.

Figure 36 shows the results for the population density of NF(a), NF(b) and HF($v \geq 2$). The optical path length is taken to be 6.5 cm. In contrast to the staged combustion results, the NF(a) excited state population density drops continuously over the viewing region. The point of maximum NF(a) concentration appears to be very close to the nozzle, and may even be inside since reaction can start taking place in the nozzle throat.

The concentration of HF($v \geq 2$) and presumably H-atoms is sufficiently high so not to limit the reactions or subsequent energy transfer. It appears from Figures 35 and 36 that the majority of reactions producing HF(v) and NF(a) are completed in the first several centimeters. The reactions which cause the temperature increase at larger values of X_c are not clear. Degradation of either HF(v), NF(b), or NF(a) internal energy to gas enthalpy is not taking place at a significant rate for $X_c > 5$ cm. The intensity of $N_2(B \rightarrow A)$ would not indicate a substantial amount of reactions are following the $N_2(B)$ production channel. One speculation could be reactions which produce NF ground state directly, and, therefore, are not observed in emission.

Another feature of Figure 36 is that the NF(a) concentration appears to level off, and indications from NF(a) spectra at $X_c > 5$ cm (where $N_2(B \rightarrow A)$ interfers with quantitative measurements) is that the NF(a) maintains a fairly constant population density out to X_c = 12 cm. The initial decrease in NF(a) is probably a geometrical effect due to the flame expansion. The NF(b) population density also maintains a fairly constant level from X_c = 5 to 12 cm after an initial drop due to decreasing HF($v \geq 2$) and gas expansion. This lack of significant decay in NF(a) and NF(b) signal again indicates the absence of fast deactivation mechanism in the chemical laser environment.

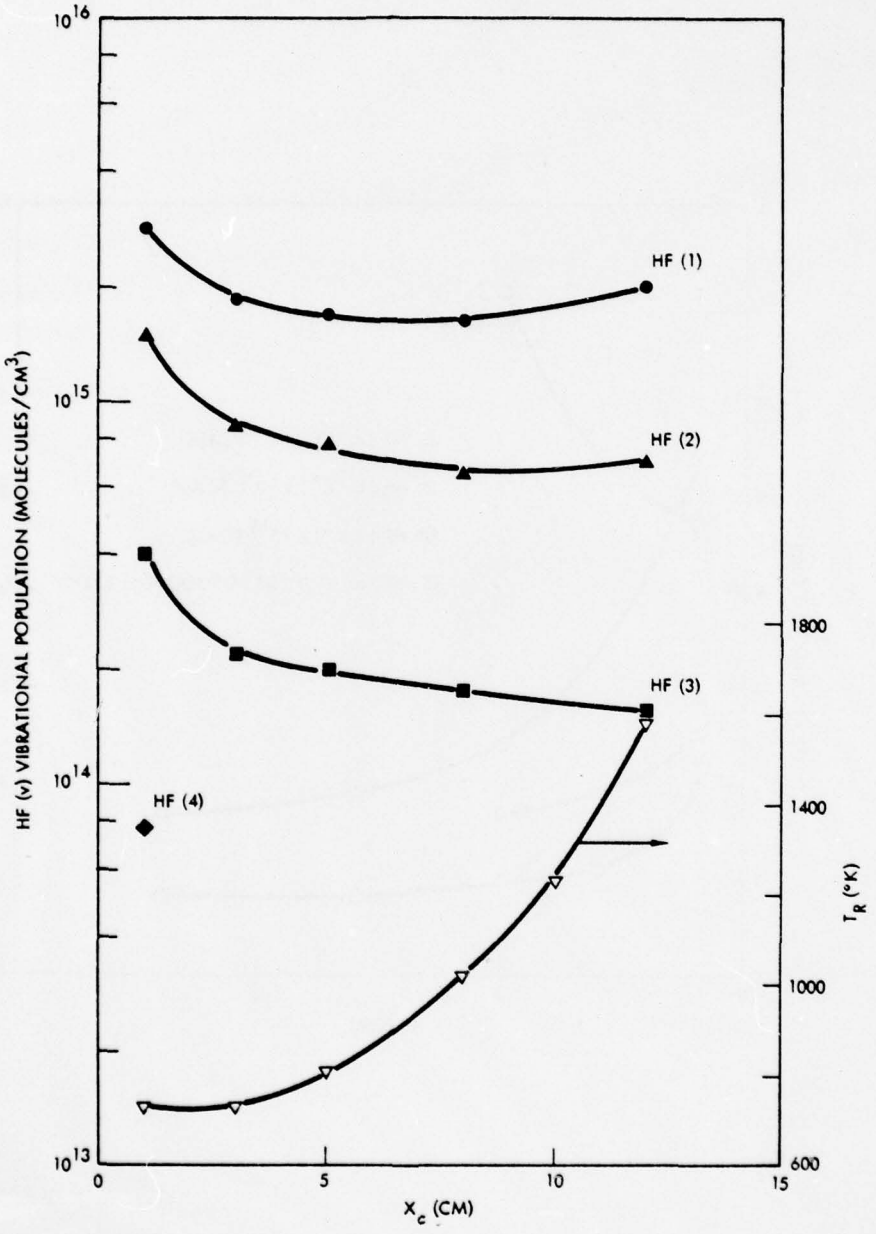

Figure 35. HF(v) Population Density and Rotational Temperature Versus X_c for Tri-Stream Nozzle Test Case.

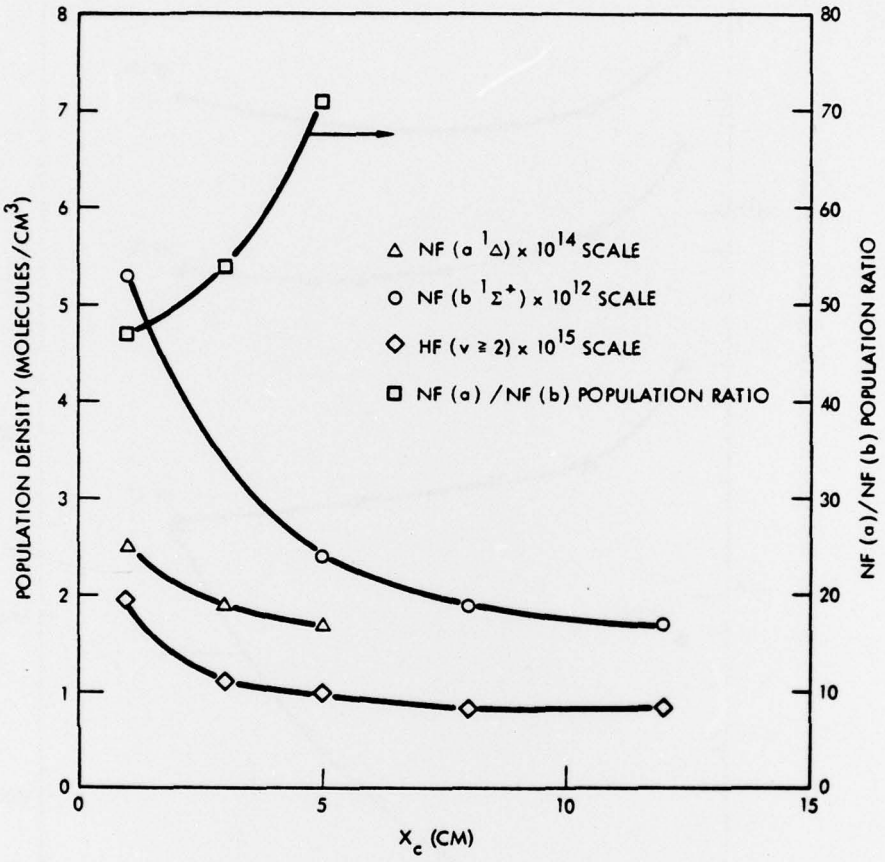

Figure 36. NF($a^1\Delta$), NF($b^1\Sigma^+$), and HF($v \geq 2$) Population Density Versus X_c for Tri-Stream Nozzle Test Case. The NF(a)/NF(b) Population Ratio Is Also Indicated in the Diagram.

Table 14 lists the results for the TSN experiments at X_c = 1.0 cm, where the highest NF* excited state concentrations are observed. The value for NF(b) population density as been adjusted by the Frank Condon factor for $\Delta v = -1$ emission intensity. A value of 2.5 cm x 6.5 cm = 16.3 cm^2 is used for the flame cross section to estimate the linear flow velocity. Again, if we assumed perfect mixing and reaction, and lack of deactivation in the flow field, the maximum amount of NF excited states would correspond to 2.3 x 10^{15} molec/cm^3. The observed amount is eleven percent of this. However, in the ideal, fully reacting case H-atoms would be the limiting reagent in the H + NF_2 reaction, so this eleven percent NF production results from only about two percent N_2F_4 dissociation.

Also shown in Figure 36 is the NF(a) to NF(b) concentration ratio. At X_c = 1.0 cm, the value of forty-three for this ratio is not close to the equalibrium ratio of six assuming HF(v = 0) is about 6 x 10^{15} molec/cm^3.

The flow speed is considerably higher compared to the staged combustion case. This is probably due to the absence of mixing blades and wedges creating drag in the flow field, as well as the absence of purge back pressure due to purge gas flow. The use of mechanical shrouds with the TSN would be expected to increase the NF(a) concentration.

3.3 CONCLUSIONS

The conclusions as given in Section 2.2.6 for the staged combustion laser are equally valid for the TSN laser, and demonstrate that many of the characteristics of the NF system are not device dependent. These conclusions include:

- Low N_2F_4 dissociation efficiency is the primary limitation for the observed NF(a) and NF(b) population density.
- NF($a^1\Delta$) and NF($b^1\Sigma^+$) are produced in an exclusively chemical reaction, laser type device.
- In a realistic chemical laser environment, the quenching of NF($a^1\Delta$) and NF($b^1\Sigma^+$) is slow.
- The NF($a^1\Delta$) concentration is factor of four higher (and the N_2F_4 flow rate per nozzle exit area a factor of twenty-three larger)[4] in the TSN experiment compared to staged combustion; the ratio of NF($a^1\Delta$) to NF($b^1\Sigma^+$) is lower in the TSN experiment.

Table 14. NF Excited State Production for the Tri-Stream Nozzle Test Case at X_c = 1.0 cm.

$NF(a^1\Delta)$	2.5×10^{14} molec/cm^3
$NF(b^1\Sigma^+)$	5.9×10^{12} molec/cm^3
$HF(v \geq 2)$	2.0×10^{15} molec/cm^3
$NF(a^1\Delta)/NF(b^1\Sigma^+)$	43/1
N_2F_4 Dissociation Efficiency	2%
Gas Pressure	1.1 torr
Gas Temperature	730°K
Linear Flow Velocity	2.5×10^5 cm/sec

- Mixing between the separate flow channels is not good in the TSN indicated by the appearance of distinct streamlines. This is in contrast to staged combustion where the flame is homogeneous.

It is somewhat surprising that the TSN did not demonstrate an improved N_2F_4 dissociation rate. The N_2F_4 is first mixed into the gas in the nozzle throat, a region of high pressure and temperature. This lack of dissociation of N_2F_4 may be partially explained by the poor transverse mixing associated with the TSN.

4. REFERENCES

1. J. A. Betts and D. J. Miller, "Advanced Laser Concepts," Air Force Weapons Laboratory Report TR-77-234, January 1978.

2. J. M. Herbelin and N. Cohen, Chem. Phys. Letters 20, 605 (1973).

3. J. M. Herbelin, D. J. Spencer, and M. A. Kwok, J. Appl. Phys. 48, 3050 (1977).

4. J. M. Herbelin, Chem. Phys. Letters 42, 367 (1976).

5. F. A. Johnson and C. B. Colburn, J. Amer. Chem. Soc. 83, 3043 (1961).

6. E. Tschuikow-Roux, K. O. MacFadden, K. H. Jung, and D. A. Armstrong, J. Phys. Chem. 77, 734 (1973).

7. M. A. Kwok, J. M. Herbelin, and N. Cohen, "Collisional Quenching and Radiative Decay Studies of $NF(a^1\Delta)$ and $NF(b^1\Sigma^+)$," TR-0077 (2940)-6, The Aerospace Corporation, April 1977.

8. Private communication, J. M. Herbelin, The Aerospace Corporation.

9. R. A. Dickerson, L. J. Zajac, and S. C. Hurlock, "Chemical Laser Advanced Nozzle Development," TR-76-45, Air Force Weapons Laboratory, June 1976.

10. R. L. Wilkins, "Vibration-Rotation Bands of HF and DF," TR-0077 (2603)-7, The Aerospace Corporation, September 1977.

11. J. T. Latimore, et.al., "H_2-Cl_2 Chemical Laser Program, Part I - CHEMLUM Code for Spectroscopic Data Analysis," Final Report Contract No. DAH01-73-C-0446, U. S. Army Missile Command, January 1974.

12. A. E. Douglas and W. E. Jones, Can. J. Phys. 44, 2251 (1966).

13. Private communication, Capt. R. Armstrong, Air Force Weapons Laboratory, Albuquerque, New Mexico.

14. W. E. Jones, Can. J. Phys. 45, 21 (1967).